CHALMERS

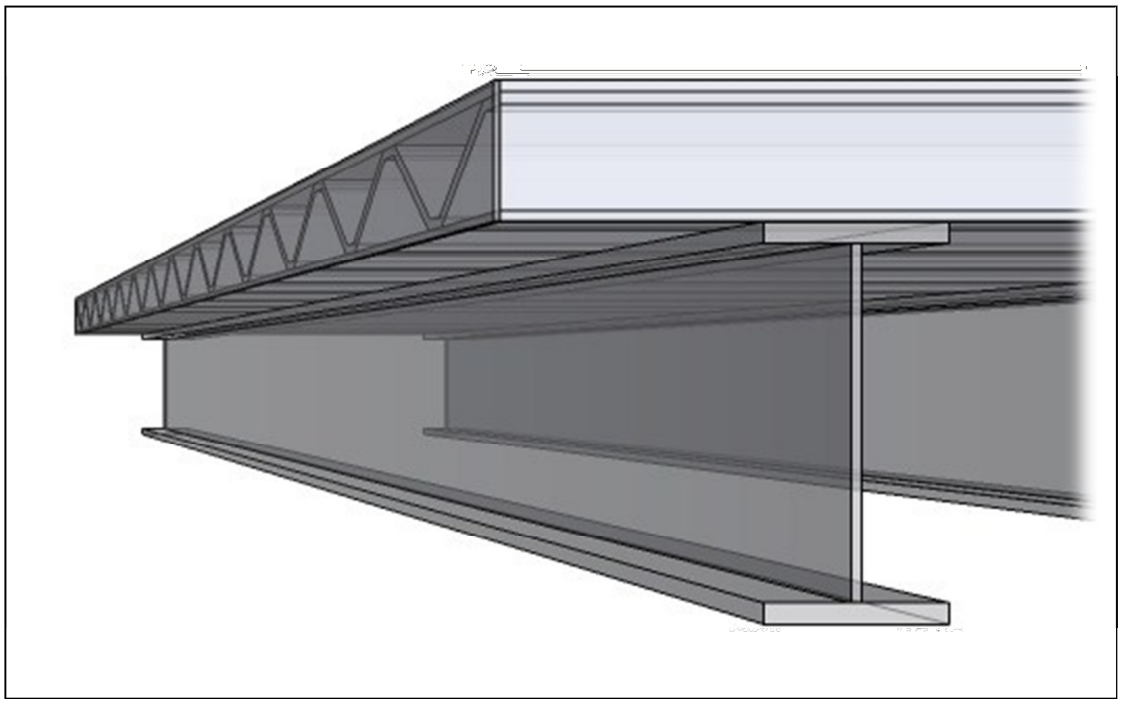

# New Concept for Industrial Bridge Construction

## Laser Welded Steel Sandwich Panels

*Master of Science Thesis in the Master's Programme Structural Engineering and Building Performance Design*

ULA ALWAN
DIANA JÄRVE

Department of Civil and Environmental Engineering
*Division of Structural Engineering*
*Steel and Timber Structures*
CHALMERS UNIVERSITY OF TECHNOLOGY
Göteborg, Sweden 2012
Master's Thesis 2012:110

MASTER'S THESIS 2012:110

# New Concept for Industrial Bridge Construction

Laser Welded Steel Sandwich Panels

*Master of Science Thesis in the Master's Programme Structural Engineering and Building Performance Design*

ULA ALWAN

DIANA JÄRVE

Department of Civil and Environmental Engineering
*Division of Structural Engineering*
*Steel and Timber Structures*
CHALMERS UNIVERSITY OF TECHNOLOGY
Göteborg, Sweden 2012

New Concept for Industrial Bridge Construction

Laser Welded Steel Sandwich Panels

*Master of Science Thesis in the Master's Programme Structural Engineering and Building Performance Design*

ULA ALWAN
DIANA JÄRVE



Examensarbete / Institutionen för bygg- och miljöteknik,
Chalmers tekniska högskola 2012:110

Department of Civil and Environmental Engineering
Division of Structural Engineering
Steel and Timber Structures
Chalmers University of Technology
SE-412 96 Göteborg
Sweden
Telephone: + 46 (0)31-772 1000

Cover:
3D-model of a half-bridge with a corrugated steel sandwich panel deck.

Chalmers reproservice
Göteborg, Sweden 2012

New Concept for Industrial Bridge Construction

Laser Welded Steel Sandwich Panels

*Master of Science Thesis in the Master's Programme Structural Engineering and Building Performance Design*

ULA ALWAN
DIANA JÄRVE
Department of Civil and Environmental Engineering
Division of Structural Engineering
Steel and Timber Structures
Chalmers University of Technology

## ABSTRACT

This thesis presents an innovative conceptual design of steel sandwich panels for the application in bridge decks with short and intermediate span lengths.

Nowadays, a critical and increasing concern in the bridge engineering is the condition of existing conventional steel bridge decks, the majority of which are deteriorated and experience extensive fatigue cracking in welded elements. The insufficient structural behaviour of conventional decks has raised a need for the development of a new deck design, which would have high structural performance, and present an economically feasible alternative to conventional decks. A number of concepts have been proposed in this field. One relatively new and promising concept that requires thorough research with regard to design and application is the steel sandwich deck.

A steel sandwich panel (SSP) is a light-weight structure, consisting of thin face sheets and a corrugated core in-between. The significant feature of this panel design is its high strength to weight ratio. The panel is not only innovative for its design but also for the technology used in manufacturing these panels. SSP is produced using an innovative laser welding technique, which is a fast and energy efficient welding procedure. Laser welding also ensures enhanced long-term performance, rapid pre-fabrication and on-site installation. The fatigue resistance of laser welds is proved to be equal to or better than that of conventional welding processes.

In this thesis the design of SSP bridge decks is performed in three steps. First, a finite element study on SSP is conducted to examine the structural performance of panels with various core configurations. The study indicated that a sandwich plate with V-core performs better compared to other studied core types, and is therefore further analysed. The effects of geometric parameters on the panel are investigated and optimum properties for the sandwich panel with V-core are selected. Finally, two bridge concepts with the optimised design of SSP are studied.

The deck design resulted in a light-weight construction, which has high strength and stiffness to weight ratios as well as good fatigue performance. The SSP is proven to have a great potential, and to be a competitive alternative to other bridge deck systems.

Key words: Laser welded steel sandwich panels, bridge decks

Nytt concept för industriell bro konstruktion

Laser svetsade sandwichpaneler

Examensarbete inom *Structural Engineering and Building Performance Design*

ULA ALWAN
DIANA JÄRVE
Institutionen för bygg- och miljöteknik
Avdelningen för Konstruktsionsteknik
Chalmers tekniska högskola

## SAMMANFATTNING

Arbetet i detta examensarbete behandlar ett nytt innovativ koncept för brodäck i stål tillverkade som sandwich paneler.

Däcket är – i allmänhet – den mest utsatta delen i en bro, så väl tillföljd av trafikbelastning och därav kommande lasteffekter, som med avseende på yttre klimatpåverkan. Dessa effekter tillsammans orsaker oftast en nedbrytning av brodäcken långt innan brons dimensionerande livslängd är uppnådd.

Brodäck i stål används endast i en begränsad utsträckning idag. De vanligaste exemplen hittas i rörliga broar och i häng- och snedkabelbroar med stora spännvidder, där fördelarna med ståldäckets höga styvhet och bärförmåga i förhållande till vikt överväger nackdelarna med denna typ av konstruktioner. Ståldäck utförs idag som svetsade ortotropa plattor. Dessa är mycket kostsamma att tillverka och underhålla och har – i många fall – visat stora problem vad gäller beständighet och utmattningslivslängd.

Erfarenheterna från ortotropa ståldäck (och till en viss del betongdäck) har på senare år motiverat omfattande forskning inom området för att hitta bättre alternativ till dessa konstruktioner. Ett koncept som på senare år har fått en del uppmärksamhet är sandwich stål panel, som kan med en viss modifiering ersätta traditionella ortotropa plattor. Ett sådant däck kan tillverkas av två stålplattor som svetsas till en korrugerad kärna i stål. Med en sådan konstruktion kan man erhålla slutna däck som ger ökad beständighet, bättre lastfördelningsegenskaper och förbättrad utmattningshållfasthet.

Tillverkningen av sandwich däck gör dessa komponenter även mer intressanta för tillämpning i brokonstruktioner. Sandwich paneler kan sammanställas med lasersvetsning, en teknik som är mycket snabbare än konventionella svetsningsmetoder och som kan ge betydligt bättre svetskvalité, och därmed bättre utmattningshållfasthet. Förtillverkade däck eller kompletta bromoduler efterfrågas också idag av brobeställaren då de underlättar ett industriellt brobyggande.

Arbetet i detta exjobb började med en omfattande litteraturstudie för att samla in de kunskapar och erfarenheter som finns inom området. Ett antal koncept för brodäck med olika konfigurationer och dimensioner studerades sedan både analytiskt och med FEM. Resultaten visar att en V-formad korrugerad kärna är effektivast ur både styvhet och bärförmåga synpunkt. Två alternativa design undersöktes i en fallstudie på en fritt upplagd vägbro. Både koncepten visade mycket tillfredsställande egenskaper. Konceptet bedöms därför ha stor potential att i framtiden ersätta konventionella brodäck.

Nyckelord: Laser svetsad sandwich panel, brodäck

# Contents

# List of Figures

# List of Tables

# Preface

This project was carried out between January – June 2012 in the Department of Civil and Environmental Engineering at Chalmers University of Technology, Gothenburg.

We would like to thank our supervisor, Associate Professor Mohammad Al-Emrani, who guided us throughout the entire writing period. We are grateful to Mustafa Aygul, Reza Haghani, and Valbona Mara for their help and assistance. We would also like to thank our course mates, who contributed to making this thesis period a fun and an interesting experience. Finally, we would like to express our gratitude to our families and friends for their support and encouragement.

Gothenburg, June 2012

Ula Alwan

Diana Järve

# Notations

*Roman upper case letters*

| | |
|---|---|
| $A_c$ | Corrugation cross-sectional area per unit width |
| $D_x$, $D_z$ | Bending stiffnesses of a beam, per unit width, associated with bending caused around x-, or z-axes, respectively |
| $D_{zx}$ | Twisting stiffness of unit-width and unit-length element cut from a plate, with edges parallel to z-, and x-axes |
| $D_{Qx}$, $D_{Qz}$ | Transverse shear stiffness, per unit width, of a beam cut from plate in the x-, and z-directions, respectively |
| $E_{xx}$, $E_{yy}$, $E_{zz}$ | Axial stiffness in x-, y, and z-directions, respectively |
| $E_z$, $E_x$ | Elastic modulus in x-, and z-directions, respectively |
| $G_{zx}$, $G_{yz}$, $G_{xy}$ | Shear modulus in x-, y-, and z-directions, respectively |
| $L$ | Length |
| $S$ | Non-dimensional coefficient in formula for $D_{Qx}$ |
| $Q_{ik}$ | Magnitude of characteristic axle load (Load Model 1) on notional lane number $i$ ($i$ = 1, 2...) of a road bridge |
| $Q_{lk}$ | Magnitude of the characteristic longitudinal forces (braking and acceleration forces) on a road bridge |

*Roman lower case letters*

| | |
|---|---|
| $2p$ | Corrugation pitch |
| $2f$ | Length of corrugation flat segment |
| $h$ | Distance between middle surfaces of face sheets |
| $h_c$ | Depth of corrugation measured from center lines |
| $l_c$ | Length of one corrugation leg measured along the centre line |
| $t_c$, $t_f$ | Thickness of core and face sheets, respectively |
| $u$ | Displacement |
| $q_{ik}$ | Magnitude of the characteristic vertical distributed load (Load Model 1) on notional lane number $i$ ($i$ = 1, 2...) of a road bridge |

*Greek lower case letters*

| | |
|---|---|
| $\alpha$ | Corrugation angle |
| $\alpha_Q$, $\alpha_q$ | Adjustment factors of some load models on lanes |
| $\nu_x$, $\nu_z$ | Poisson's ratios associated with bending caused around x-, or z-axes, respectively |
| $\lambda$ | Eigenvalue |
| $\sigma_{cr}$ | Elastic critical plate buckling stress |

*Abbreviations*

| | |
|---|---|
| SPS | Sandwich Plate System |
| SSP | Steel Sandwich Panel |
| LBW | Laser Beam Welding |
| L/GMAW | Hybrid Laser Gas-metal Arc-welding |
| PC/QA | Process Control and Quality Assurance |

# 1 Introduction

## 1.1 Background

For the past 40 years, the design of steel decks has almost remained unchanged and mainly decks consisting of a top deck plate supported by longitudinal stiffeners and transversal crossbeams has been used (1). These so-called orthotropic decks experience fatigue cracking in different welded elements, mainly because of the fatigue critical details, and constantly raising traffic loads. Concrete decks in composite bridges are also very critical elements which are subjected to direct load effects and harsh environmental conditions. In practice, these decks are renovated or in some extreme cases totally replaced in periods of 20-30 years.

In general, total replacement of a whole bridge due to deck degradation is neither needed nor an economically feasible solution. The main load-carrying elements in the bridge are usually in good condition. Bridge re-decking is therefore the solution often adopted. There is a clear need for new bridge deck concepts, which are cost-effective and at the same time provide high structural performance. These concepts should also preferably be manufactured with a high degree of prefabrication to provide rapid on-site installation process.

Many different bridge deck concepts have been discussed and investigated over the years. One relatively new and promising concept that requires thorough research with regard to manufacturing, design and application is the sandwich steel deck system. A sandwich system is a light-weight prefabricated element consisting of two steel face plates and a core in-between. The core can have various materials and geometrical configurations. One of the possible designs is the sandwich plate system (SPS) that has an injected elastomer as a core. Another solution is the automated laser welded all-steel sandwich panel (SSP) that has a steel core of various types.

The development of SPS started in 1997 by the company Intelligent Engineering (IE). The primary application of these sandwich plates was in the ship industry. Advantages of SPS in ship construction industry encouraged its use in civil engineering applications, for example in bridges decks. The other concept, the SSP, has been investigated less than SPS mainly due to manufacturing issues. SSP requires special fabrication because traditional welding techniques, such as arc welding cannot be applied on the thin plates, which are usually used in the core. Today, the most suitable welding technique to produce sandwich plates is laser welding. However, since laser welding technology was not properly developed until recently, the utilisation of laser welding was limited. This in turn prevented and put on hold further advances of all-steel sandwich panels for years. The recent breakthroughs in laser welding, and particularly in hybrid-laser welding technology have opened new possibility to develop and further investigate the application of steel sandwich plates in construction.

## 1.2 Project Aim

The aim of this thesis is to investigate the possibilities offered by the light weight and high stiffness of sandwich plate panels for the application in bridge structures.

## 1.3 Method

The work in this thesis started with a thorough literature study on both concepts, the SSP and the SPS panel. Based on the outcome of the literature study, the most promising design concepts are selected for a more thorough analysis.

Numerical analyses with the finite element method are performed to obtain an overview of the structural behaviour and the load carrying capacity of sandwich steel panels. Also, a parametric study is performed using available analytical solutions (Reissner-Mindlin plate theory) to determine the most efficient design of the element. The finite element modelling is conducted with Abaqus/CAE software.

## 1.4 Outline of Thesis

Chapter 1 gives introduction to the thesis, and describes the purpose of this work.

Chapter 2 is a detailed literature study of two sandwich systems: sandwich plate system (SPS) and steel sandwich panels (SSP). The chapter starts with a short history of sandwich plates, describes previously conducted researches, then continues to present the advantages of each panel, and finally describes the production process. In the end, the most promising concept of the sandwich system to be further investigated is chosen.

Chapter 3 continues with a study of different core configurations, where various steel sandwich panels are assessed in terms of their stiffness, and finally the core with best structural properties is chosen.

Chapter 4 presents a more detailed investigation on the behaviour of the chosen core design. Parametric study is conducted to choose the best geometric parameters for the core.

Chapter 5 is a finite element analysis on a bridge with a sandwich panel deck.

Finally, conclusions and recommendations for future research are presented in Chapter 6.

## 1.5 Limitations

The work performed in this thesis is of a more conceptual nature, even though detailed analytical and numerical studies have been carried out. All the chosen geometries are preliminary, no detailed design of connections is performed, and several simplifications in bridge structures are made, such as the effect of edge beams on the response of the bridge deck is neglected. The main emphasis in the work was devoted to the bridge deck, and therefore other supporting structures, for instance main girders or stiffeners are not thoroughly investigated.

# 2 Literature Study

## 2.1 Sandwich plate system

### 2.1.1 History

Initially sandwich plate system (SPS) was developed to replace traditional stiffened steel plates in offshore structures subjected to heavy loads in Canadian Beufourt Sea. Since 1997, the company Intelligent Engineering (IE) has been driving the development of SPS panels, and IE is known as the main manufacturer of SPS, especially for ship reparations. The benefits of SPS in ship construction industry encouraged its use in civil engineering applications, for example in bridge decks and floors (2).

According to Momčilović (2009) sandwich plate system is recognized as a lightweight material due to the low density of the core ($\gamma=1,1g/cm^3$). SPS consists of two steel plates, which work as a flange, and an injected elastomer core that functions as a web (see Figure 1- 1). The elastomer core transfers shear between two face plates dissipating strain energy over a big area, which results in the reduction of load concentrations, and therefore leads to smaller permanent deformations (3). SPS has very high flexural stiffness and strength to weight ratio. The elastomer core provides a continuous support for the panel, therefore there is no requirement for having closely spaced longitudinal stiffeners as conventional orthotropic plates (see Figure 1- 1 (b)). Due to the continuous support provided by the core local buckling of steel plates is prevented (2).

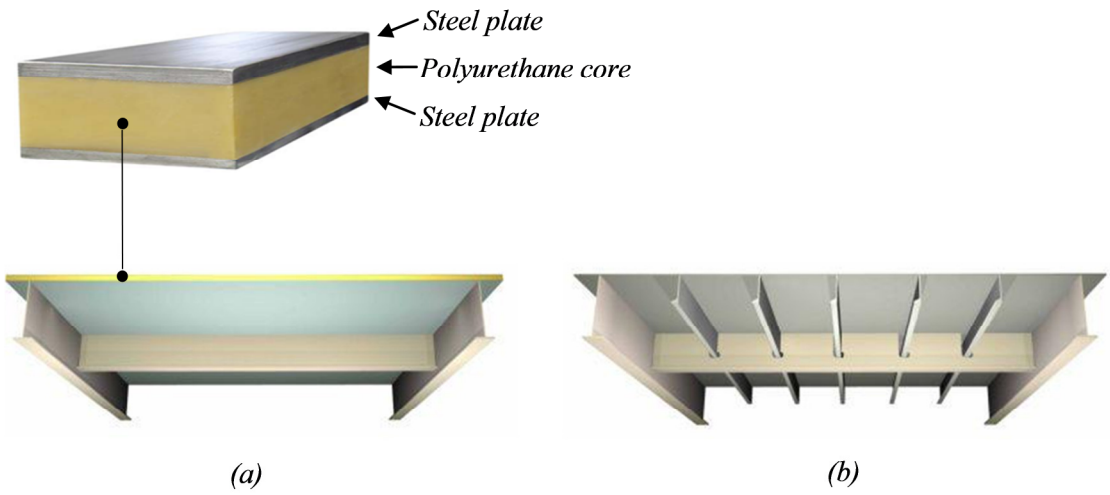


*Figure 1- 1(a) bridge deck with SPS structure, (b) conventional orthotropic steel deck with longitudinal stiffeners (3)*

Intelligent Engineering carried out three static tests on a 5-40-5 mm SPS bridge deck in Ludwigshafen, Germany, where SPS was used as a replacement of the traditionally stiffened bridge deck plate . The dimensions 5-40-5 mm were the thickness of the top steel plate, the elastomer core and the bottom steel plate, respectively. The results showed that the load carrying capacity of the sandwich plate was 1.29 times the design load applied at the maximum eccentricity. Fatigue test revealed that sandwich plate panel subjected to 5 million load cycles experienced no development of cracks.

Also, finite element analyses were carried out in ANSYS software. The estimated deflection showed a difference of 7% between the experimental and estimated values. Strain results were acceptable, without any significant differences between the experimental and the analytical model, and no creep was observed during on-site tests. IE concluded that 5-40-5 sandwich plate system can be considered as an acceptable design and it achieves better properties compared to the stiffened steel plate deck (4).

An example where the sandwich plate system panel has been applied is the Shenley Bridge in Ontario, Canada. SPS with dimensions 6.4-38-6.4 mm was placed on three steel plate girders as shown in Figure 1- 2. The connection between SPS panels was made by first bolting the webs of transverse angles to each other with ASTM A325 (see Figure 1- 2). Secondly, the longitudinal angles were bolted to the top flange of the support girder (see Figure 1- 3), and then a groove weld was carried out along the top of the adjacent transversal joint to ensure complete connection between panels (see Figure 1- 3 (3)).

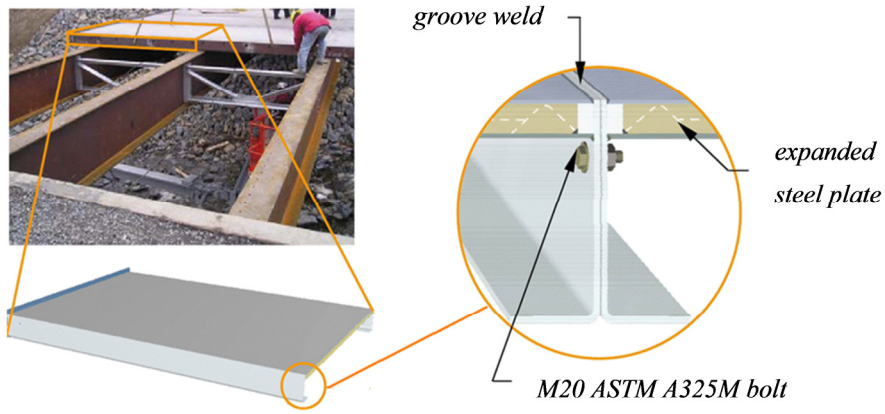


*Figure 1- 2 Shenley bridge in Ontario (7)*

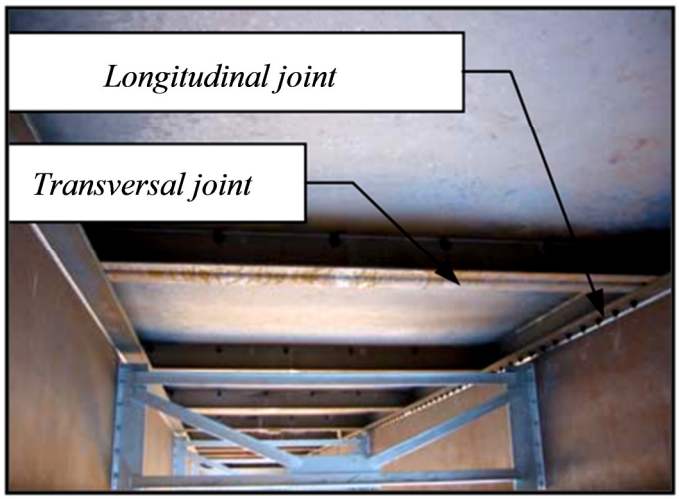


*Figure 1- 3 Shenley bridge in Ontario (7)*

## 2.1.2 Production of sandwich panels

### 2.1.2.1 SPS panels

The first step is the preparation of panels, which involves cutting the face plates to the required dimensions, cleaning the surface to achieve a required surface roughness and cleanliness, placing iron perimeter bars on top of the lower plate, and finally welding the bars along the corners (see Figure 1- 4). Also, elastomer locks have to be fastened on the lower panel – they keep the elastomer in place. Second step is to assemble the lower and upper plate either by hydro welding or conventional welding. Third step is the injection of elastomer core through pre-drilled injection holes on one side of the panel. To control the amount of elastomer, overflow holes on the opposite side are used (Figure 1- 5 (b)). To avoid distortion or deformation of plates during the hardening process of elastomer, heavy load is placed on the face plate; see Figure 1- 5 (a). Elastomer is hardened in five hours after injection is completed (3). Final step of production is to drill holes inside the panel for future installation purposes. After this, the injection holes are sealed by welding, as shown in Figure 1- 6.

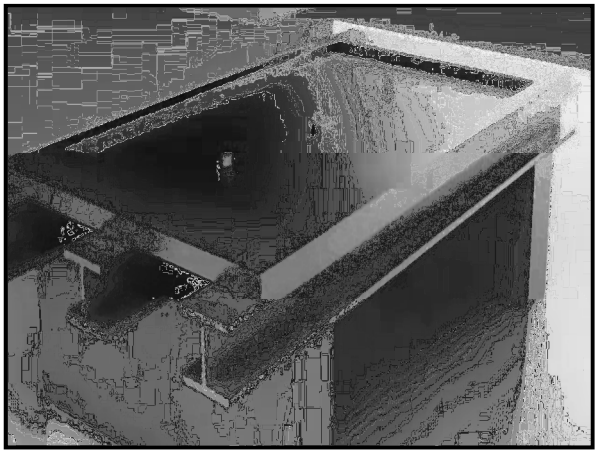

*Figure 1- 4 Locks made of elastomer placed on the lower plate (3)*

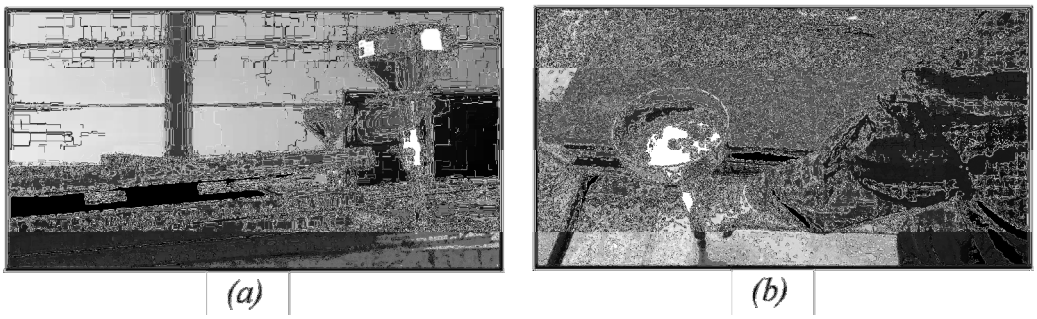


*Figure 1- 5 (a) heavy load place on the panel, (b) elastomer flows out from overflow hole (3)*

*Figure 1- 6 Overflow holes and injection holes sealed by welding (3)*

### 2.1.3 Application of SPS

#### 2.1.3.1 Bridge deck replacement

The light weight of SPS helps to reduce the dead load of bridge decks by with up to 70% compared to a concrete deck – this benefit of SPS allows bridges to carry a greater live load without a need for additional girders. When the deck of existing bridges is replaced with SPS deck, load restrictions can be removed and extra lanes added to increase traffic capacity. Replacement of the deck can be achieved by connecting SPS panels with existing steel or concrete girders on site, or if rapid replacement is a critical factor, then the whole deck can be replaced with preassembled longitudinal deck-girder units. The replacements process takes a very short time due to the simplicity of the process and easy-installation features of SPS panels, therefore bridges can be partially used during the maintenance, which leads to minimal distribution of traffic (3).

An example of simple and fast installation of SPS panels is the Dawson Bridge in Edmonton, Canada. It was a 100 year-old and a 5-span truss bridge with a combination of concrete and timber deck. The bridge was not able to carry the design load anymore, and therefore the deck was replaced using SPS construction, which increased the life-span of the bridge for another 100 years (3).

#### 2.1.3.2 Bridge strengthening with SPS Overlay

SPS Overlay is used to strengthen steel bridge decks. The first strengthening with SPS Overlay method was performed on vehicle decks on ships. Later it was developed further to strengthen bridges. A degraded steel bridge deck is strengthened by adding an overlay of a stiff SPS plate without the need of removing the existing structure. SPS Overlay uses the existing deck as a bottom or top plate, depending on which part of the deck has to be strengthened. The elastomer core and the new steel plate will be then added to form a new SPS deck.

The deck with SPS Overlay reduces concentration of wheel loads, improves fatigue resistance, and increases the service life of a bridge (3). Also, the cost of construction is reduced, because as mention previously, the existing deck is kept in place. In addition to this, the bridge can be operational throughout the construction period (3).

### 2.1.3.3 SPS Overlay

SPS Overlay application consists of four main steps (3). The first step is removing the existing wearing surface and clearing the whole deck by means of grit blasting so that in the end only the surface of steel plate is visible, see Figure 1-8 (a). The second step is to connect perimeter bars to the existing bridge deck by means of welding. A special elastomer lock is placed on the clean surface of the deck. Then, a new top plate is placed and welded or adhered to perimeter bars to ensure airtight cavities – this avoids leakage of elastomer. Third step is the injection of elastomer into the cavities. During injection, a restrained beam is used as shown in Figure 1- 7 (c) to avoid possible deformations of the new plate during the hardening process of elastomer. Final step is to add a new wearing surface to the repaired bridge deck, see Figure 1- 7 (d).

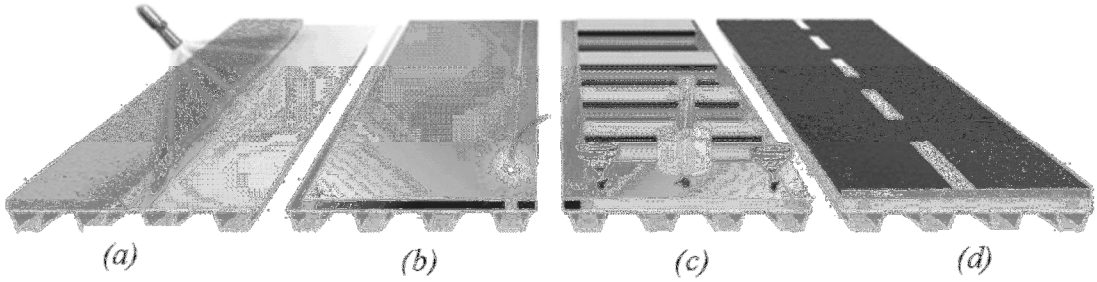


*Figure 1- 7 SPS Overlay production: (a) cleaning of the existing steel bridge, (b) welding of the new plate to parameter bars, (c) injection of elastomer, (d) final result (11)*

When using SPS Overlay, the distribution of wheel loads is much better, resulting in a better fatigue life, because critical stresses are decreased. As shown in the report of Intelligent Engineering, the stresses in the weld joints are reduced from 42 MPa to 16 MPa, see Figure 1- 8 (3).

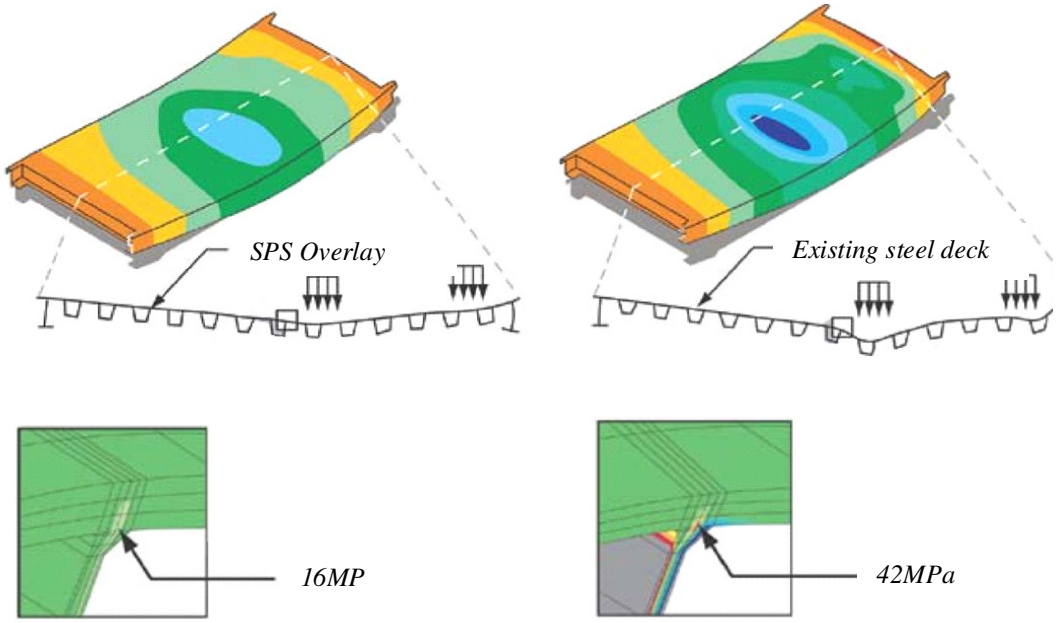


*Figure 1- 8 Comparison of stresses in a joint of a deck with SPS Overlay and an existing steel deck with through stiffeners (3)*

An example of SPS Overlay application is the Mafang Bridge in China (1984), built of a bolted and welded box girder superstructure with orthotropic deck, which consists of two lanes that are 920 m in length and 9 m in width. It was required to strengthen the bridge without closing the traffic and keeping the deck weight to a minimum, therefore SPS was the best choice to strengthen this orthotropic bridge deck. Another use of SPS Overlay was the Schönwasserpark Bridge in Germany (1972) with orthotropic bridge steel deck that carried very busy motorway over a rail line. SPS Overlay was used as a strengthening method for the deck when bridge showed signs of fatigue. The SPS Overlay project was completed in 16 days (3).

The Huskisson Canada Passage Bridge, 50m long and 6m wide, in Liverpool UK was also strengthened using SPS Overlay in year 2006. The design load of the bridge had to be increased to carry heavy loads of excavators and a 93 tonne face shovel. A new 8mm thick steel plate, 20 mm elastomer and the existing steel plate were used in the SPS Overlay process. During 9 days, 300 $m^2$ of the bridge deck were strengthened. The bridge was partially used during the work process, it was only closed completely for two hours per day (3) (5).

### 2.1.4 Advantages of SPS

#### 2.1.4.1 Simplicity

Elastomer core provides a continuous support to the plates, therefore the need for transversal stiffeners in the bridge deck is reduced, saving significantly on the material cost, and decreasing the amount of welding. Construction time is simplified, because the SPS panels are prefabricated and delivered on site. When the SPS Overlay system (see Chapter 2.1.3.2) is used, there is no need to remove the existing deck – this saves time on construcion and installation (6).

#### 2.1.4.2 Performance

Elastomer core spreads strain energy over a large area, and therefore decreases load concentrations. This results in the reduction of deformations, and avoids crack formations. Another important advantage is the weight – SPS is considered a lightweight material; it gives 50% weight reduction for bridge decks enabling longer spans in bridges. Compared to conventional stiffened plates, the fatigue and corrosion resistance of a bridge deck with SPS panels is higher because of the reduced amount of welds (6).

#### 2.1.4.3 Safety

SPS has a very high resistance to fire. It has a built-in fire protection, and does not need any additional insulation, which is normally the requirement in steel structures. The reason for this is the elastomer core, which is an effective insulator against heat (7). SPS structure has a smaller amount of sensitive connection details, resists crack propagation, and absorbs high loads – this leads to an increasing resistance to accidental loads (6).

#### 2.1.4.4 Cost

The advantages of SPS, such as simplicity of installation, the reduced number of secondary stiffeners and connection details, increased fatigue and corrosion resistance, reduction in construction time, and high fire resistance result in a lower construction cost. Moreover, the maintenance of SPS is simple and fast, therefore the cost reduces even more in the long run (6).

## 2.2 Steel sandwich panel

### 2.2.1 History

History of sandwich-like panels dates back to 1950's, when first proposals for construction of such elements were made (8). However, fabrication of all-steel sandwich panels was not feasible, because laser welding technology suitable for panel production was not yet well-established and the cost of high-power laser sources was very expensive. Therefore, other types of sandwich panels, for example sandwich-plate-system products or fibre reinforced polymer composite sandwich panels were being developed and applied in structures instead (9).

The increased use of all-steel sandwich panels in civil, mechanical and other industrial sectors has started approximately 20 years ago. The main application of panels back in the time was in shipbuilding industry. In the late 1980's, U.S. Navy developed the first all-steel sandwich element consisting of two metal sheets laser fused to a corrugated metal core for application in marine transport. In 1994 this concept was first implemented on the ship USS Mt. Whitney (10). Panels showed excellent structural behaviour, and the installation saved 40% in weight compared to conventional stiffened plate structures. However, the research and application of panels was abandoned as no manufacturing process that could produce panels with a reasonable price was yet available (11).

The behaviour and production analysis of panels have been performed also in countries like Great Britain, Germany and Finland. For example, German shipyard Meyer Werft has conducted research on sandwich-like panels. Other institution to be mentioned is the Ship Laboratory of Helsinki Technical University that initiated a research in 1988 with regard to the application of sandwich panels in shell structures of an icebreaker (8). As stated in the report of Hoffart (2008), a panel design aimed for the use in double hull structure of intercoastal tankers was tested and the results showed a 73% higher crash resistance, at the same time when the hull depth was decreased by 2/3. Other researchers have reported a weight saving of 30-50% compared to conventional panels when used in high-speed vessels (11).

Prior to the use of steel sandwich panels in superstructures it should be possible to estimate the structural performance of such elements both, analytically and numerically. For estimating structural response of laser-welded sandwich plates the most reasonable approach is sandwich plate theory, where the plate is homogenized with respect to stiffness. Other methods, which use an idealised mathematical model of the structure become too time-consuming, when various design alternatives have to be analysed (12). First structural analyses of the general concept of sandwich panels with various materials were conducted 70 years ago, when panels were aimed for the use in aeronautical industry. Theoretical foundations were described in literature more explicitly starting from the 1970's (13). After that numerous authors have formulated

theories for the calculation and analysis of sandwich structures. The most recent works to be mentioned are the five papers by Romanoff et al. (see: (14), (15), (16), (17), (18)), where the authors carried out theoretical basis for sandwich plates with respect to bending response, patch loading and the stiffness of welded T-joints. Also commercial softwares are available for the analysis and design procedures of different core type metal sandwich panels, one of them being ESAComp software developed by a Finnish company Componeering Inc. (www.componeering.com). Many of this existing engineering data and design procedures can be implemented in the design of all-steel laser welded sandwich panels.

### 2.2.2 Types

Sandwich panels function similarly as an I-beam, in which plates resist bending and the core resists shear forces. Also, the geometry of the core determines the level of isotropy of a panel. Therefore, cross-section of the core is an essential element in a panel and for that reason has to be designed properly. Various configurations of cores are available and are illustrated in Figure 1- 9 and Figure 1- 10.

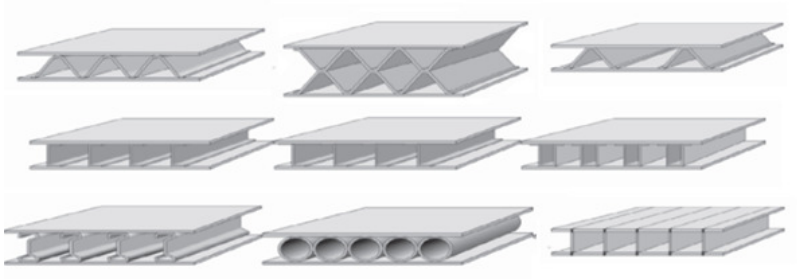

*Figure 1- 9 Sandwich panel types depending on various core shapes (19)*

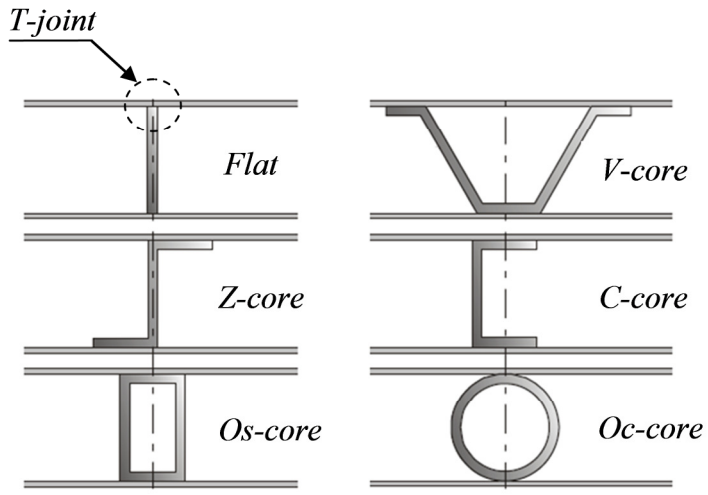


*Figure 1- 10 Sandwich panel types (13)*

Many authors have described the advantages of one or other core geometry. The simplest core is a flat core, which consists of face plates and a perpendicular flat web plate (18), see Figure 1- 11. Connection between the plates is laser-based and denoted

as T-joint. Distance between the web-plates is usually 10-100 times the thickness of face plates. This type of panel is highly orthotropic, since the stiffness of the panel varies in different directions.

According to Caccese & Yorulmaz (2009) prismatic cores are preferred in SSP as they are easy to fabricate and possess high longitudinal stiffness. Some core geometries, however, have other advantages, for example X-core, which has a bigger capacity to absorb energy. Telford (2006) states that triangulated web profiles improve the transverse stiffness considerably. Pantsar & Salminen (2004) conducted quality and cost analysis of laser welded O-core and V-core sandwich panels. The results showed that O-type sandwich structures do not bend as much as V-cores during welding and they also have a high nominal stiffness, therefore it is easier to perform welding. However, O-type panels weigh more. Hoffart & Hansen (2008) have written that the most common core is a corrugated structure.

Telford (2006) suggests that hot-rolled I-section (see Figure 1- 11) is a cost-effective solution for a core profile because of its stability during assembly. Compared to fully triangulated profile, I-section requires almost no preparation before fabrication, this making it more economic to produce.

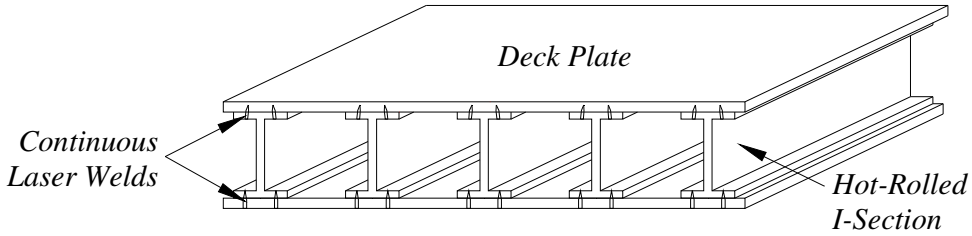


*Figure 1- 11 SSP panel with I-section (1)*

### 2.2.3 Advantages

Conventional steel decks with closed-through stiffeners are highly orthotropic, this leading to possible load concentrations within the stiffeners and furthermore to fatigue damages. A more even distribution of loads and a considerable increase of transversal stiffness could be achieved by adding a lower plate to the construction, and this is exactly what a steel sandwich panel design includes. As SSP consist of upper and lower plates, the neutral axis is situated in the mid-depth of the panel. This results in a much better structural efficiency, since both plates are at maximum distances and are fully stressed (20).

Telford (2006) presents a comparison between a conventional 3.6m span deck and a 4.5m span sandwich panel deck. The analyses are presented in Table 1- 1, from which it can be denoted that longitudinal bending stresses are significantly smaller in the sandwich plate, because of its higher section modulus and a better load distribution in transversal direction, see Figure 1- 12, where longitudinal stresses for the symmetric bridge panels under centred wheel load are presented. As seen from Table 1- 1, sandwich panels are slightly heavier than equivalent conventional steel decks. However, as SSP can span longer distances this additional mass could be decreased by the reduction of required cross girders within the bridge structure, or by omitting them at all. On average cross-girders give 25-35% additional mass to a closed through orthotropic steel deck (20).

*Table 1- 1 Comparison of structural performance (1)*

| Deck type | Closed through orthotropic deck | Sandwich panel |
|---|---|---|
| Longitudinal span | 3600 *mm* | 4500 *mm* |
| Second moment of area (per m width) | 1.1x108 $mm^4 / m$ | 4.3x108 $mm^4 / m$ |
| Mass/ $m^2$ (average) | 150 $kg / m^2$ | 290 $kg / m^2$ |
| Max displacement under 2x20 *kN* wheel loads | 1.60 *mm* | 0.75 *mm* |
| Span: displacement ratio | 2250:1 | 6000:1 |
| Max longitudinal bending stress:<br>a) in deck plate<br>b) in lower flange/trough | <br>– 33 $N / mm^2$<br>+ 55 $N / mm^2$ | <br>– 25 $N / mm^2$<br>+15 $N / mm^2$ |
| Max web bending stress | ± 34 $N / mm^2$ | ± 25 $N / mm^2$ |
| Max transverse bending stress:<br>a) hogging stress in deck plate<br>b) sagging stress in deck plate | <br>+ 100 $N / mm^2$<br>– 59 $N / mm^2$ | <br>+75 $N / mm^2$<br>– 50 $N / mm^2$ |

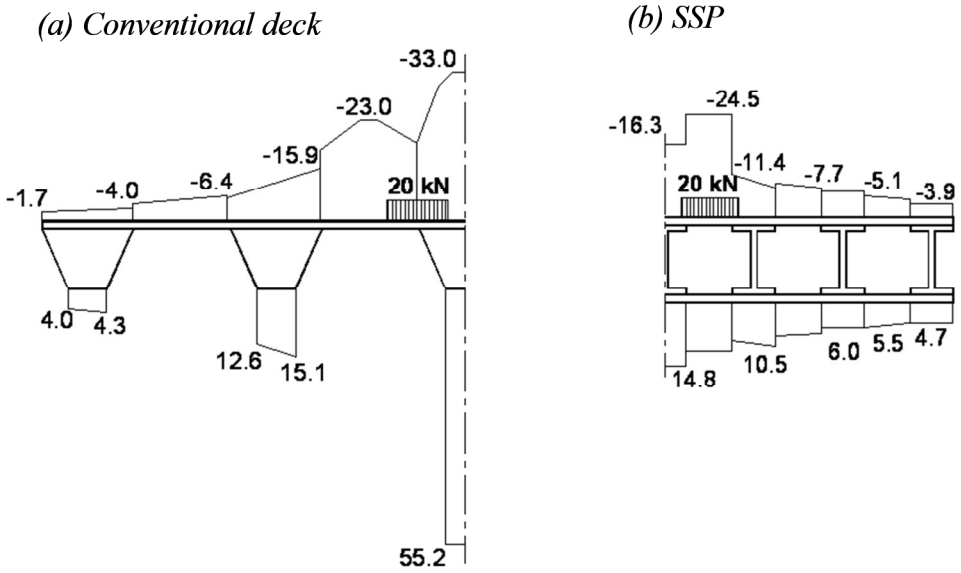


*Figure 1- 12 Comparison of mid-span longitudinal stresses (N/mm$^2$) when wheel-load is in the middle for (a) conventional deck, and (b) SSP of I-sections (1)*

Another major advantage of sandwich-constructions is their production. Panels are factory made and delivered on site, also the assembly of panels is fast and easy, therefore disruption of road or railroad traffic can be prevented. According to the SANDWICH (2000) project, erection time is reduced by 30% (21).

Fatigue performance of steel sandwich structures is significantly better than of conventional bridge decks, where extensive fatigue cracking can occur in the deck-to-cross girder joins, web-to-deck joints and in the surfacing of the decks (20). These types of fatigue damages can be prevent with the new laser welding technology used for the production of sandwich panels.

### 2.2.4 Production process

Sandwich steel plates comprise of thin components, therefore conventional welding techniques for panel fabrication cannot be applied, otherwise this can lead to heat distortions, which in turn cause fatigue problems (11).

A manufacturing technology, which is suitable for SSP fabrication is laser beam welding (LBW) that has been developed already from the 1960's. Nevertheless, the use of lasers was possible starting from the 1990's, when advances in laser technology emerged (22), such as greater power, better beam quality, development of real-time closed-loop process control and automated quality assurance system, weld monitoring, and control of all critical welding parameters (9). Comparison and advantages of laser welding with competing techniques were presented by Miller (1980) and are summarised in Table 1- 2.

*Table 1- 2 Advantages of laser welding (23)*

| Competing Process | Advantages of Laser Welding |
|---|---|
| Gas Metal Arc | Faster welding rates; low distortion; no filler metal required |
| Submerged Arc | Faster welding rates; low distortion; no flux or filler needed |
| Electron Beam | No need to be performed in a vacuum; on-line processing; shorter cycles and higher uptimes; does not require radiation shielding |

Although laser welding offers many advantages over conventional welding, some disadvantages also exist, for instance because of the small focus-diameter of lasers, the weld gap bridgeability is very limited. A solution to overcome possible drawbacks in LBW would be the combination of the new laser technology and the well-established arc welding – this combination of technologies is called hybrid laser gas-metal arc-welding (L/GMAW). Merging of laser process with other welding types could also be possible, however these combinations have not been actively researched nor utilised yet. A major recognition of laser-hybrid welding technology dates back to 2000, when Meyer Werft opened a new panel line for the welding of deck and bulkhead panels using $CO_2$ lasers (22). By exploiting the advantages of both technologies a much better weld joint is achieved. The comparison of main characteristics of the two processes separately and combined are shown in Figure 1-13.

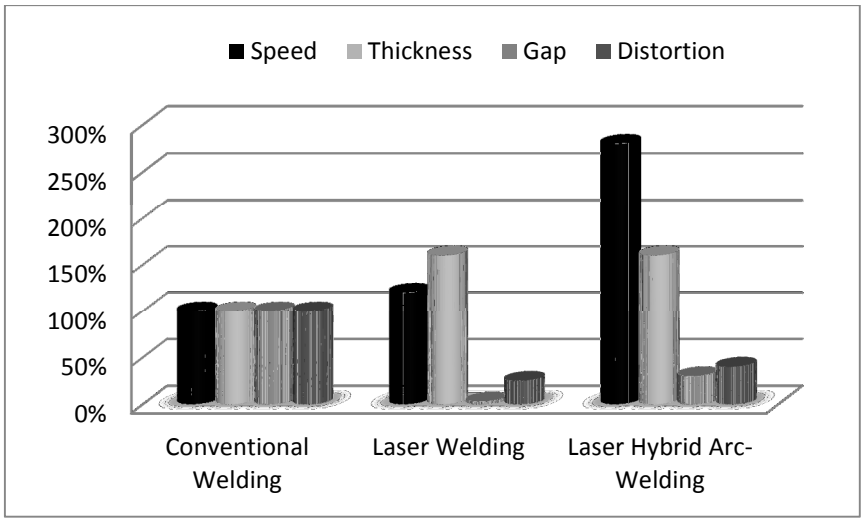


*Figure 1- 13 Principle comparison of welding methods and their characteristics (11).*

L/GMAW is proved to be three to ten times faster than conventional welding (24). High welding speed not only saves time and money, but also leads to less heat input resulting in a small heat affected zone. This in turn provides less weld distortion and the fatigue life of a welded joint is therefore improved. For even a more efficient and feasible manufacturing of structures a welding process control denoted as Process Control and Quality Assurance (PC/QA) system was developed in the year 2000. With PC/QA the welding process is monitored in real-time and all possible defects are being identified and repaired. The difference of weld quality with closed-loop control and without is presented in Figure 1- 14. This technological innovation eliminates the need for human visual inspection and makes L/GMAW a reliable, accurate and cost-effective manufacturing technology (10).

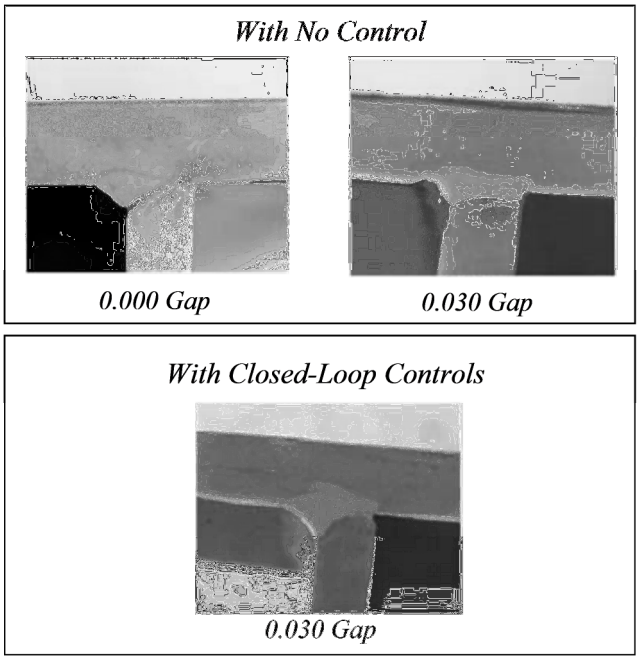


*Figure 1- 14 Welded T-joint with Gap Variations (9)*

The process through which SSP components are joined together is referred to as the *keyhole* technique; it creates deep penetrations compared to conventional welding type (see Figure 1- 15), even though laser has no direct access to the web material.

Flange to web connection in SSP is performed such that the heat of laser beam penetrates through the full-section of the upper plate and into the underlying inner core, after which plates become rigidly joined because of the immediate cooling of the weld (1). A schematic illustration of the L/GMAW process is presented in Figure 1-16.

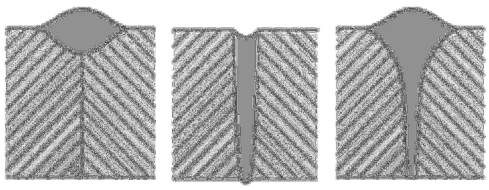

*Figure 1- 15 Difference between Gas Metal Arc Welding (GMAW), Laser and Hybrid Laser Welding welds(25)*

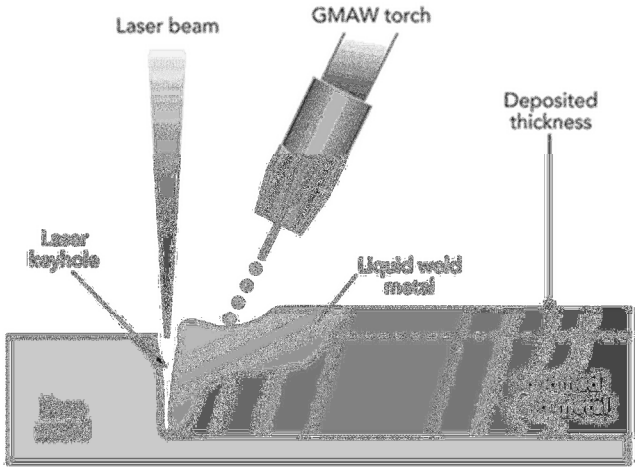


*Figure 1- 16 Hybrid laser welding process (22)*

#### 2.2.4.1 Fatigue performance of laser welds

Fatigue resistance of laser welds is proved to be equal to or better that that of conventional welding processes (10). Multiple tests have been carried out by various researches on the fatigue performance of welded joints.

One important factor influencing fatigue life of the welds is their geometry. Caccese et al. (2006) described the results of fatigue studies, which were performed to investigate the influence of geometry on fatigue life of laser-welded T-joints. With hybrid laser welding it was possible to manufacture smooth, nearly circular geometric profiles, which resulted in fatigue life higher than that of traditional welds. A set of tests was performed on a cruciform hybrid-laser welded specimen equipped with a real-time feedback control of the weld process. The results were compared to historical data provided by Munse et al. (1983) for laser welded T-joints, and by Kihl (2002) for conventional welded steel cruciforms with the same material. The results showed a much higher fatigue life for hybrid-laser welded details (see Figure 1- 17) and also improved geometric profiles that were almost circular.

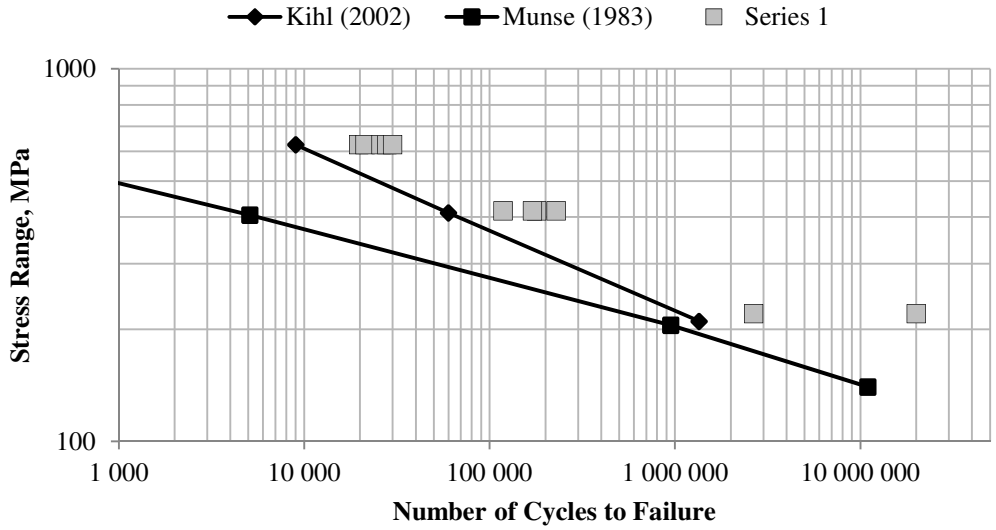


*Figure 1- 17 Fatigue test results (10)*

The above mentioned tests reflected the local fatigue response only. To provide a more realistic assessment of fatigue performance of laser-welded sandwich panels, Bright and Smith (2004) conducted tests on laser welded bridge deck components with an I-core geometry. First test was a web bending test, which represented bending that might occur under offset wheel loads. Second one was a deck bending fatigue test under direct wheel loads, see Figure 1- 18.

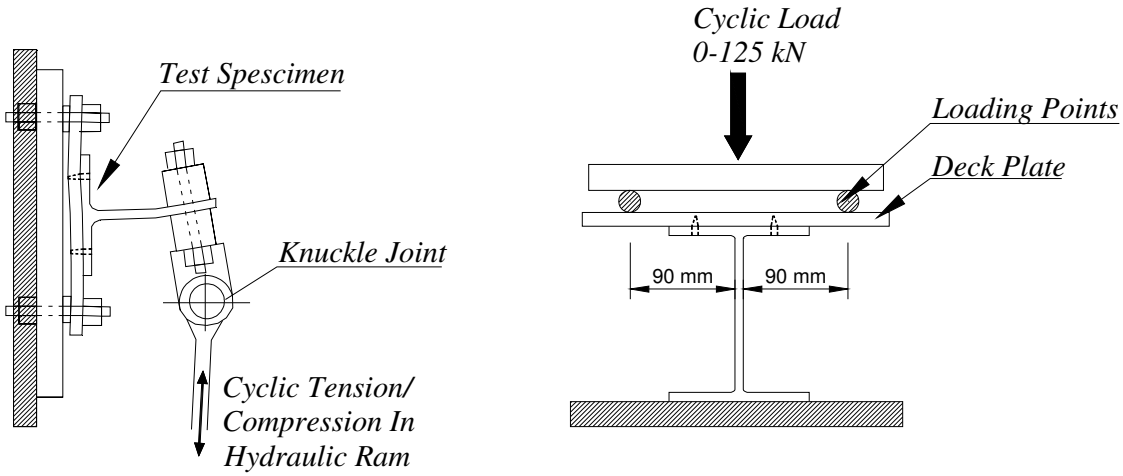


*Figure 1- 18 Fatigues tests, on the left – web bending test; on the right– deck bending test (1).*

During the web bending test no weld failures were observed, all fatigue failures occurred in the parent metal of the web, thus SSP design offers outstanding fatigue durability when subjected to web bending stresses. The second test, where shear stresses taken by the weld are the most significant ones showed satisfactory results. Eventually shear stresses can cause fatigue failures, however a much better weld performance was noticed than that of a similar classic weld joint used in conventional steel decks (1).

### 2.2.5 The chosen concept

After thorough literature study, it was decided to continue with a detailed research of the all-steel sandwich panel. Reasons for this choice are as follows:

- the durability of the elastomer core material in long term performance is questionable;
- steel sandwich panel has a much higher strength and a better structural performance than the sandwich plate system, for instance, connection between steel plates and the core for sandwich plate system is made through bonding, which has much less strength than a welded connection;
- there is lack of existing data about the behaviour of the steel sandwich panels on bridges.

# 3 Study of different core configurations

## 3.1 Introduction

The method used in this chapter is finite element modelling (FEM), which is performed in the software Abaqus/CAE. The aim of Chapter 3 is to study sandwich plates with various core geometries, and to choose the most promising concept, which could be further analysed and optimised for the use in a bridge deck.

The structural behaviour of a sandwich plate is related to its stiffness, since the load carrying capacity of the plate increases as its stiffness increases. The sandwich plate analysed in this thesis is represented in Figure 1- 19. It consists of two face sheets and a core in between. This type of plate exhibits different behaviour in the transversal and longitudinal directions. In the direction of the corrugation, the core contributes to resisting shear forces and bending moments, and therefore the stiffness in the z-direction is much higher than that in the x-direction. Thus, the right choice of the core configuration is important for the overall panel behaviour.


*Figure 1- 19 Steel sandwich plate*

Figure 1- 20 presents ten different core configurations that were studied in terms of their axial, shear and bending stiffnesses in x- and z-directions using Abaqus/CAE S8R shell elements. The amount of core material in each panel was kept constant, in this way the results were comparable to each other.

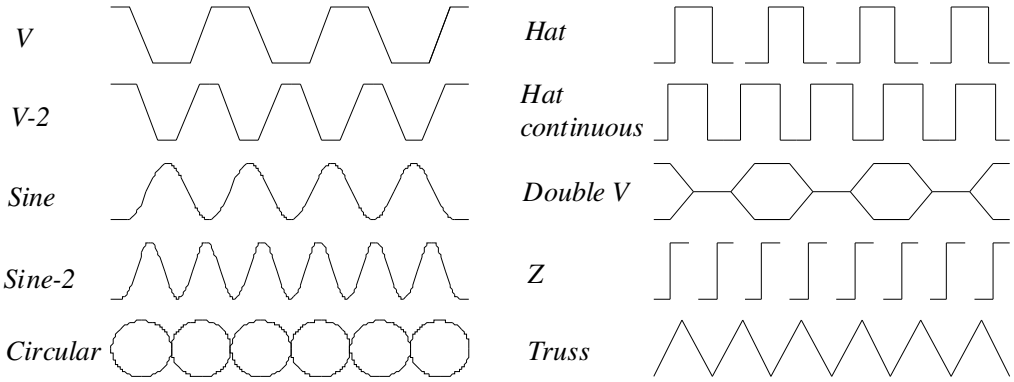


*Figure 1- 20 Analysed corrugated core types*

## 3.2 Axial stiffness

For axial stiffness along the x-axis, horizontal displacement of 1 mm in the x-direction was applied on one of the side plates as shown in Figure 1- 21. The second side plate was restrained in x-direction, and the bottom edges of both side plates were

prevented from movement along the y-axis. Plate movement was also prevented in z-direction.

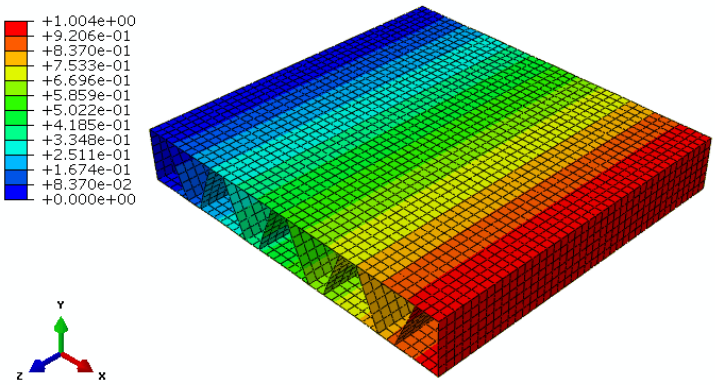


*Figure 1- 21 Displacement in x-direction*

To obtain the axial stiffness in the direction perpendicular to the corrugation, a vertical displacement of 1 mm in the y-direction was applied on the top plate. The bottom plate was restrained from movement in the y-direction, and the edges of bottom and top plates were restrained in x-direction (see Figure 1- 22).

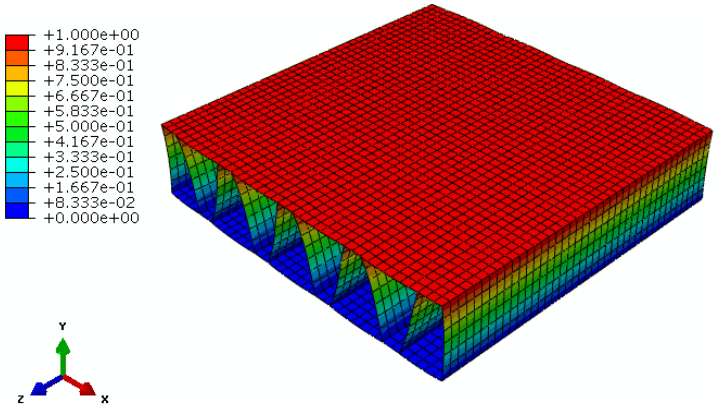


*Figure 1- 22 Displacement in y-direction*

To obtain axial stiffness in the z-direction, displacement of 1 mm in the z-direction was applied on one side of xy-plane, which was also prevented from movement along the y-axis. Other side was restrained in z- and y-directions, and the plate was restrained in x-direction (see Figure 1- 23).

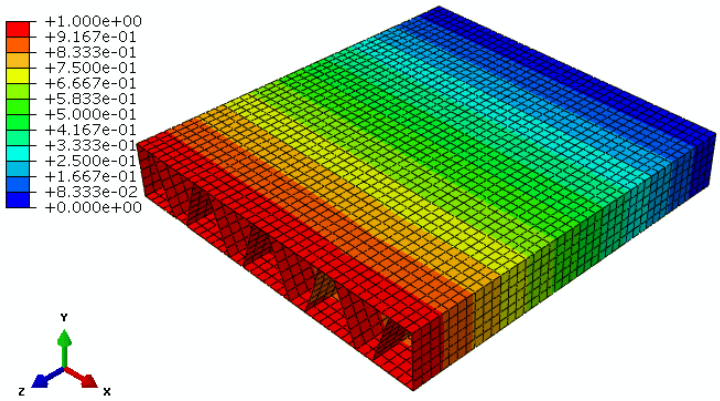


*Figure 1- 23 Displacement in z-direction*

With a prescribed displacement $u$, and the reaction force obtained from FE analysis, axial stiffness $E$ can be calculated from the following equation:

$$E = \frac{F}{u} \tag{1}$$

## 3.3 Shear stiffness

The shear stiffness in x-direction was calculated by subjecting the top plate of the panel to surface traction of 1 N/mm$^2$ in x-direction. The bottom plate was restrained in x-directions, the edges of top and bottom plates were restrained along the y-axis, and the side plates were restrained in z-direction (see Figure 1- 24).

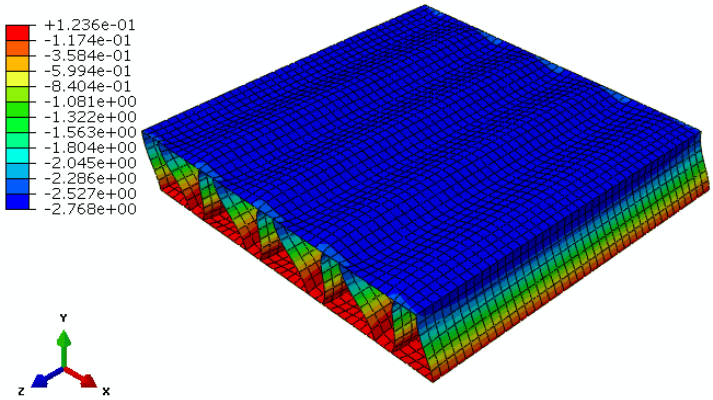


*Figure 1- 24 Displacement in x-direction*

Similarly, for shear stiffness along the z-axis, surface traction of 1 N/mm$^2$ was applied in the direction of z-axis. The bottom plate was restrained along the z-axis, the edges of top and bottom plates were prevented from movement along the y-axis, and side plates were restrained from movement in x-direction (see Figure 1- 25).

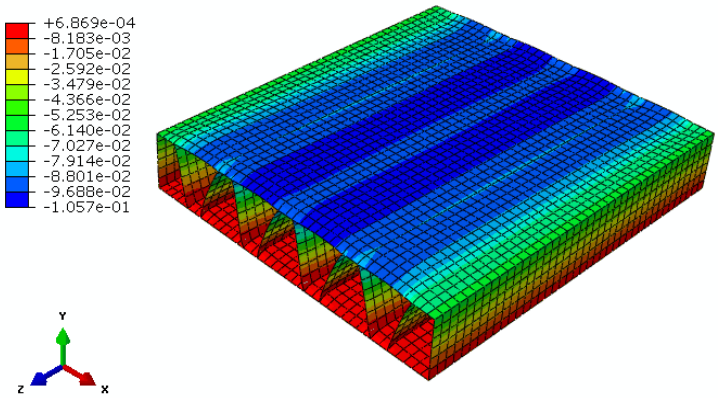


*Figure 1- 25 Displacement in z-direction*

With a prescribed surface traction $\tau$, the panel height $h$, and the displacement obtained from FE analysis, shear stiffness $G$ can be calculated as follows:

$$G = \frac{\tau}{u} \cdot h \tag{2}$$

## 3.4 Bending stiffness

Bending stiffness of the panel was calculated from the following equation:

$$D = \frac{5qL^4}{384u} \tag{3}$$

where $L$ is the panel length, $q$ is the load, and $u$ is the displacement obtained from FE analysis. The panel was subjected to a distributed load of 1 MPa, and the boundary conditions were simply supported. Deflections caused by moments around the x- and z-axis were obtained from FE analysis, and bending stiffnesses for both cases were calculated according to Equation (3). Representation of results obtained from FE analysis is in Figure 1- 26 and Figure 1- 27.

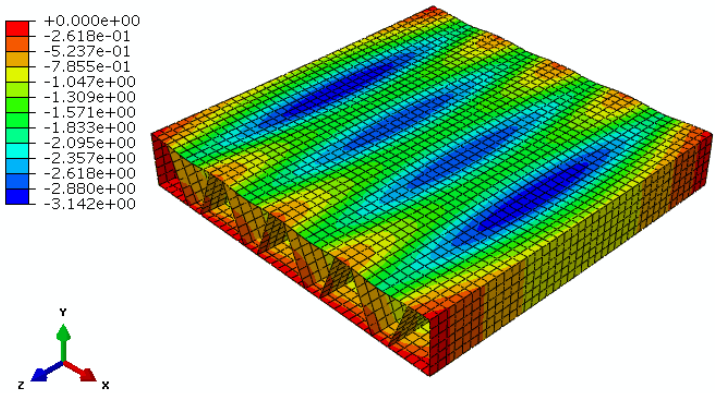


*Figure 1- 26 Deflection caused by the moment around x-axis*

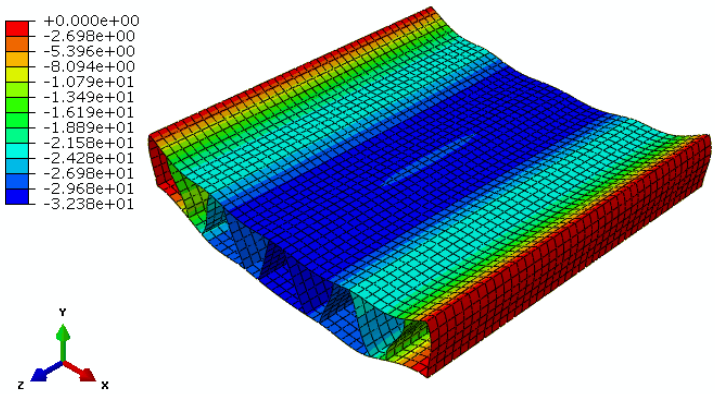


*Figure 1- 27 Deflection caused by the moment around z-axis*

## 3.5 Results

The results obtained from finite element analyses are presented in Table 1- 3. When comparing axial stiffness $E_{xx}$ in x-direction, the difference between core types is small. This is due to the negligible contribution of the core to the stiffness along the x-axis. However, a drastic difference can be observed for the stiffness $E_{yy}$ in y-direction, where not only plates contribute to resisting the loads, but also the core has a significant impact on the stiffness. The shear stiffness along the corrugation is much higher than that in the transversal direction. This is also represented with the results, where the difference between $G_{yz}$ and $G_{yx}$ is at least 23% for the truss, and in the other cases more than 90%. Similarly, the contribution of the core to the bending caused by the moment around x-axis is higher, resulting in a high bending stiffness.

Interesting observation is between the truss core and the V-core. Both cores have a similar triangular configuration; the only difference is the flat segment of corrugation (see Figure 1- 28). Even though this difference is small, it does have a great influence on the shear stiffness. This can be explained as follows, the forces in V are transferred mainly through the webs by truss action, where the webs of one unit are in tension and compression. This results in a force couple, which in turn creates local moments, and high shear forces in the flanges. Such force couple is not present in the truss core, which makes its behaviour in shear action much better. As seen in Figure 1- 29 and Figure 1- 30, the local moment in the upper and lower flanges of the V core causes very high deflections compared to the truss. From this observation, it is clear that the length of the horizontal part of the corrugation has to be as small as possible. Truss core cannot be chosen as a concept because of the fabrication issues, therefore the best core would be V with a minimum horizontal part, which only has to fulfil the length requirements necessary for laser welding (min 10 mm, max 20 mm). From the results presented in this chapter, it was decided that the most promising core concept is V, which will be subsequently analysed in more details.

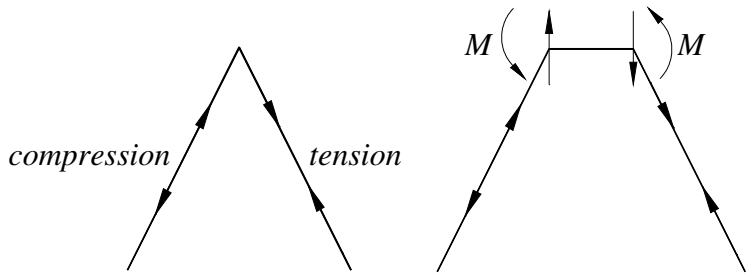


*Figure 1- 28 Transfer of forces in the truss core and the V-core*

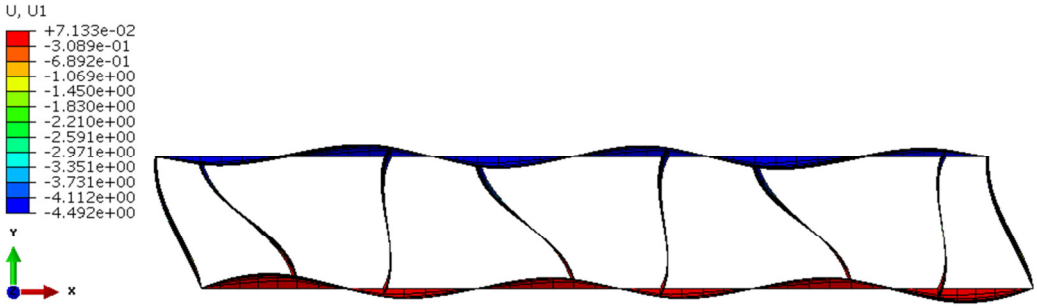


*Figure 1- 29 V-core in shear action*

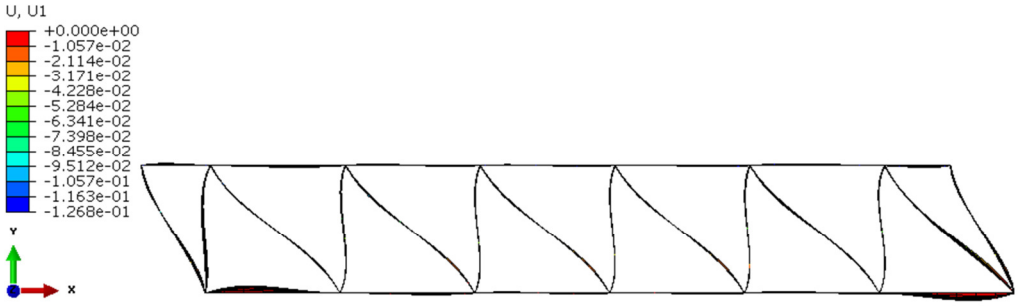


*Figure 1- 30 Truss core in shear action*

*Table 1- 3 Results*

| Core type | Axial stiffness | | | Shear stiffness | | Displacement | | Bending stiffness | |
|---|---|---|---|---|---|---|---|---|---|
| | $E_{xx}$ [N/mm] | $E_{yy}$ [N/mm] | $E_{zz}$ [N/mm] | $G_{yx}$ [N/mm$^2$] | $G_{yz}$ [N/mm$^2$] | $u_z$ [mm] | $u_x$ [mm] | $D_z$ [Nmm] | $D_x$ [Nmm] |
| V | 5.00E+06 | 8.06E+07 | 7.62E+06 | 56.66 | 1.84E+03 | 53.9 | 2.00 | 1.54E+09 | 4.17E+10 |
| V-2 | 4.82E+06 | 9.07E+07 | 7.59E+06 | 93.70 | 2.46E+03 | 30.9 | 1.80 | 2.69E+09 | 4.62E+10 |
| Sine | 4.42E+06 | 3.74E+07 | 7.62E+06 | 140.29 | 1.30E+03 | 14.9 | 3.58 | 5.59E+09 | 2.32E+10 |
| Sine -2 | 4.39E+06 | 4.39E+07 | 7.62E+06 | 151.11 | 1.78E+03 | 11.6 | 2.76 | 7.17E+09 | 3.02E+10 |
| Circular | 4.33E+06 | 2.87E+07 | 7.63E+06 | 10.07 | 5.87E+02 | 109.0 | 28.0 | 7.66E+08 | 2.97E+09 |
| Hat | 5.20E+06 | 9.67E+07 | 7.62E+06 | 6.98 | 2.06E+03 | 163.0 | 1.87 | 5.11E+08 | 4.45E+10 |
| Hat - continuous | 5.19E+06 | 1.00E+08 | 7.62E+06 | 5.72 | 2.40E+03 | 190.0 | 1.80 | 4.37E+08 | 4.62E+10 |
| Double V | 4.89E+06 | 4.49E+07 | 7.62E+06 | 15.60 | 1.34E+03 | 83.8 | 2.87 | 9.93E+08 | 2.90E+10 |
| Z | 5.11E+06 | 1.00E+08 | 7.64E+06 | 7.45 | 2.31E+03 | 154.0 | 1.80 | 5.41E+08 | 4.62E+10 |
| Truss | 4.00E+06 | 9.90E+07 | 7.62E+06 | 2000.00 | 2.60E+03 | 1.70 | 1.63 | 4.90E+10 | 5.11E+10 |

# 4 Optimization and analysis of V-core configuration

## 4.1 Introduction

In this chapter optimisation study for the V-core configuration is performed to investigate the effect of the geometric parameters on the stiffness of the panel. From obtained results an optimum design for the V corrugation is chosen. Optimisation is carried out by homogenising the sandwich structure with respect to its stiffness into an equivalent 2-D plate. This procedure prevents excessive computational time compared to when idealised mathematical model of the structure is used. The 2-D model is validated through finite element analyses by comparing the bending response of a complete 3-D SSP model and the equivalent 2-D model.

## 4.2 Equivalent 2-D plate

Stiffness of the sandwich structure depends on the geometric parameters presented in Figure 1- 31. These relevant parameters affecting the behaviour of the panel are as follows:

$2p$ - corrugation pitch

$\alpha$ - corrugation angle

$t_c, t_f$ - thickness of core and face sheets, respectively

$h$ - distance between the face sheets from centreline

$h_c$ - depth of the core

$2f$ - length of corrugation flat segment

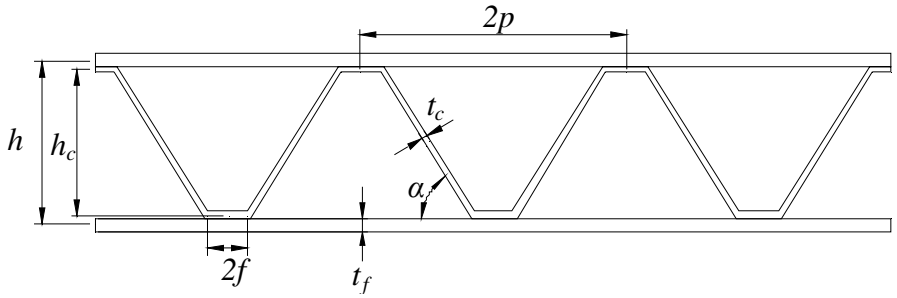


*Figure 1- 31 Parameters of a V-core sandwich panel*

One possibility to study the effects when varying these parameters is to create multiple 3-D finite element models. However, this procedure is time consuming, and therefore another method is applied, namely the 3-D panel will be reduced to an equivalent homogenous 2-D continuum by applying the Reissner-Mindlin plate theory. To further simplify the calculations only a unit width of a panel is studied with a corrugation pitch *2p*, see Figure 1- 32 (a). For this type of conversion seven physical constants, which would represent a 2-D model are required. These constants include the bending stiffness $D_x$ and $D_z$, a twisting stiffness $D_{xz}$, the transverse shear stiffness

$D_{Qx}$ and $D_{Qz}$, and the Poisson ratios $\upsilon_x$ and $\upsilon_z$ (see Figure 1- 32 (b). By calculating elastic constants for varying geometric parameters behaviour of the SSP can be studied. The elastic constants representing a 2-D continuum have been derived by Libove and Hubka (26), and the derivation of these constants is discussed in Chapter 4.3.

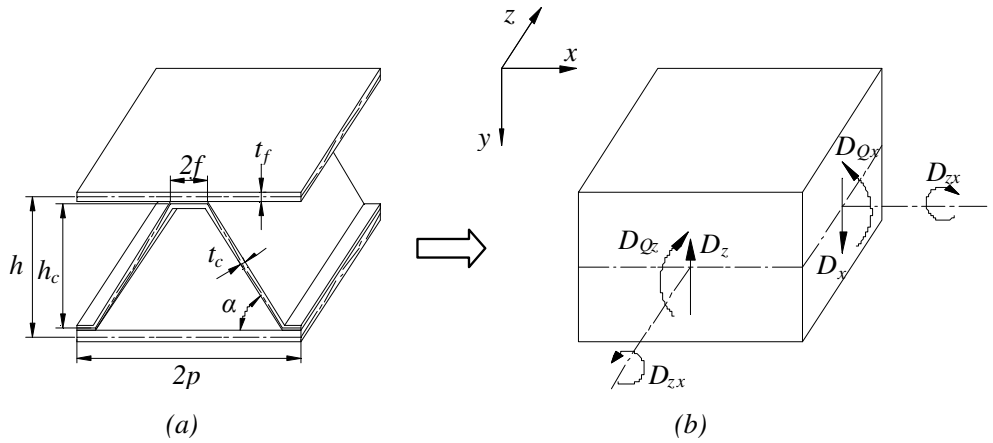


*Figure 1- 32 (a) dimensions of a unit, (b) equivalent elastic constants of a 2-D plate*

This approach for analysing steel sandwich panels has been previously used by many authors, and has also been experimentally verified. Chang et al. *(27)* studied the bending behaviour of corrugated-core sandwich plates, where the 3-D sandwich panel was reduced to an equivalent 2-D thick plate. The elastic constants were computed using the expressions from Libove and Hubka *(26)*. The bending behaviour obtained from the analytical solution was compared to experimental testing and a complete 3-D model of the sandwich plate with same dimensions described in the report of Tan et al. *(28)*. The deflection obtained by Chang et al. agreed closely with the deflections reported by Tan et al.

Zangani et al. *(29)* evaluated the stiffness for Z-cored sandwich panels with a polymeric foam in-between. The elastic constants were computed by transforming the panel into an equivalent 2-D plate. Lok et al *(30)* introduced a sandwich panel with a truss core and studied its elastic stiffness using the equations from *(26)*. The only difference between the truss core and the corrugated core is that the truss core has two inclined plates in a panel unit, whereas the corrugated core is continuous through the whole length. The accuracy of the method when transforming a 3-D model into a 2-D model has been reported in previous works on sandwich panels, therefore this approach will also be applied in this thesis.

## 4.3 Elastic constants

### 4.3.1 Bending and twisting stiffness

The bending stiffness $D_z$ and $D_x$, and twisting stiffness $D_{zx}$ are obtained from following expressions:

$$D_z = E(I_c + I_f) \tag{4}$$

$$D_x = \frac{EI_f}{1-\nu^2\left(1-\frac{EI_f}{D_z}\right)} \tag{5}$$

$$D_{zx} = 2GI_f \tag{6}$$

where:

$I_c$ - moment of inertia, per unit width, of corrugation cross-sectional area, $m^3$

$I_f$ - moment of inertia, per unit width, of face sheet cross-sectional area, $m^3$

$\nu$ - Poisson's ratio of face sheet material

### 4.3.2 Transverse shear stiffness

The transverse shear stiffness in planes parallel to the corrugation can be expressed as:

$$G_{Qz} = \frac{Gt_c h^2}{pl_c} \tag{7}$$

where:

$$A_c = \frac{l_c t_c}{p}$$

$A_c$ - corrugation cross-sectional area per unit width, m

$l_c$ - length of one corrugation leg measured along the centre line

The transverse shear stiffness in planes perpendicular to the corrugation axis can be obtained as:

$$G_{Qx} = Sh\left(\frac{E}{1-\nu^2}\right)\left(\frac{t_c}{h_c}\right)^3 \tag{8}$$

where:

$S$ - non-dimensional coefficient depending upon the core shape and is obtained from Equation (9). The major simplification in calculation of $G_{Qx}$ is that the radius between the contact area of face sheets and the core is assumed to be zero, this simplifies Equation (9), for detailed calculations refer to APPENDIX A**.**

$$S = \frac{6\frac{h_c}{p}B_1B_4 + \left(\frac{p}{h_c}\right)^2}{12 - \left[-2\left(\frac{p}{h_c}\right)^2 B_2 + \frac{h_c}{h}\left[6B_4\left(B_1B_3 - B_2{}^2\right) + \left(\frac{p}{h_c}\right)^3 B_3\right] + \frac{h}{h_c}\frac{p}{h_c}B_1\right]} \tag{9}$$

### 4.3.3 Verification

Verification is performed in Abaqus/CAE on V-core steel sandwich panel of width $a = 1590\,mm$, and length $b = 1590\,mm$. This panel will be modelled as a complete 3-D sandwich panel, and an equivalent 2-D orthotropic thick plate. The V-core unit has following dimensions: $p = 265mm$, $f = 82.5mm$, $d = 250\,mm$, $t_f = 10mm$, $t_c = 8mm$.

First step was to create a complete 3-D model of the sandwich structure by inserting material properties presented in Table 1- 4. This sandwich panel was modelled with simply supported boundary conditions on four edges. A uniformly distributed load of $q = 20N/mm^2$ was applied. Subsequently, deflection in the bottom of the flange was obtained.

Second step was to calculate elastic constants for the equivalent plate according to equations in Chapter 4.3; detailed calculations are presented in APPENDIX A. These elastic constants will be converted into orthotropic material properties using following expressions (31):

$$E_z = \frac{12D_z}{d^3} \qquad E_x = \frac{12D_x}{d^3} \tag{10}$$

$$G_{zx} = \frac{6D_{zx}}{d^3} \qquad G_{yz} = \frac{D_{Qz}}{kd} \qquad G_{xy} = \frac{D_{Qx}}{d} \tag{11}$$

$$\nu_z = \nu_x \frac{D_x}{D_z} \tag{12}$$

where:

$k$ - is the shear correction factor, taken as 5/6

This conversion is necessary for assigning material properties to the 2-D plate in Abaqus/CAE. Afterwards, the orthotropic plate was modelled as a 1590mm wide, 1590mm long plate, and meshed with SHELL elements of thickness 250mm. Plate was modelled with the same loading and boundary conditions as the complete 3-D panel, but with the equivalent material properties (see Table 1- 4).

*Table 1- 4 Material properties and elastic constants*

| **3-D FE model. Original material properties** | **Equivalent elastic constants** | **2-D FE model. Equivalent material properties** |
|---|---|---|
| $E = 210MPa$<br>$\nu = 0.3$ | $D_z = 1.01 \cdot 10^{11}\,N \cdot mm$<br>$D_x = 7.72 \cdot 10^{10}\,N \cdot mm$<br>$D_{zx} = 5.80 \cdot 10^{10}\,N \cdot mm$<br>$D_{Qz} = 4.03 \cdot 10^{5}\,N/mm$<br>$D_{Qx} = 4.37 \cdot 10^{3}\,N/mm$<br>$\nu_x = 0.3$<br>$\nu_z = 0.23$ | $E_z = 6.27 \cdot 10^{4}\,N/mm^2$<br>$E_x = 4.81 \cdot 10^{4}\,N/mm^2$<br>$G_{zx} = 1.81 \cdot 10^{4}\,N/mm^2$<br>$G_{yz} = 1.83 \cdot 10^{3}\,N/mm^2$<br>$G_{Qx} = 1200kN \cdot m$<br>$\nu_x = 0.3$<br>$\nu_z = 0.25$ |

Deflections were obtained and compared with those acquired from 3-D finite element model. Deflections from 3-D and 2-D FE analysis are 33.2 mm and 32.6 mm,

respectively. The results show very good agreement; discrepancy between the results is 1.8%. Representation of models is presented in Figure 1- 33.

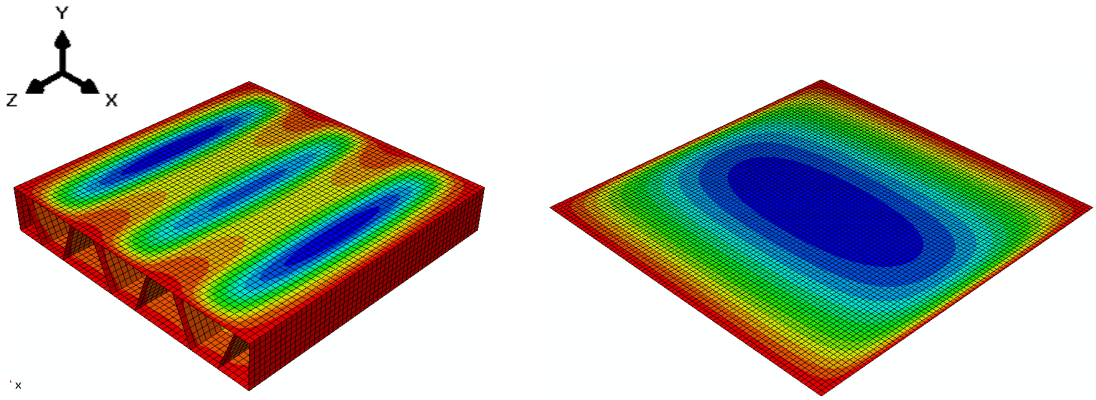


*(a)* *(b)*

*Figure 1- 33 (a) deflection results for complete 3D panel, (b) deflection results for complete equivalent 2D plate*

### 4.3.4 Results

Results obtained from the parametric study are presented in Table 1- 9 in APPENDIX B. In this study core height $h_c$, flange thickness $t_c$, and the amount of core material was kept constant. The corrugation angle varied from 50° to 85°. Main observation from the results was that with an increasing ratio of core height divided by the core thickness $\frac{h_c}{t_c}$ the stiffness of the panel decreases. This is because the core plate becomes thinner, and therefore the stiffness of the panel decreases as well. Also, when increasing the ratio of the corrugation pitch divided by core height $\frac{p}{h_c}$ the stiffness of the panel decreases due to a decreasing amount of corrugations for a given plate width, this making the structure less stiff. Finally, it was observed that the change in angle has a very high effect on the shear stiffness. When increasing the angle, bending stiffness $D_x$ and $D_z$ change only marginally, as can be seen in Table 1- 9**.** However there is a significant drop in shear stiffnesses (see Figure 1- 34 and Figure 1- 35), especially for the shear stiffness $D_{Qx}$ between angle 50° and 60°.

Conclusions made after the parametric study are that $\frac{p}{h_c} < 1$, the angle has to be between 50…60 degrees, and from Chapter 3 it was decided that horizontal part of the corrugation has to be as small as possible.

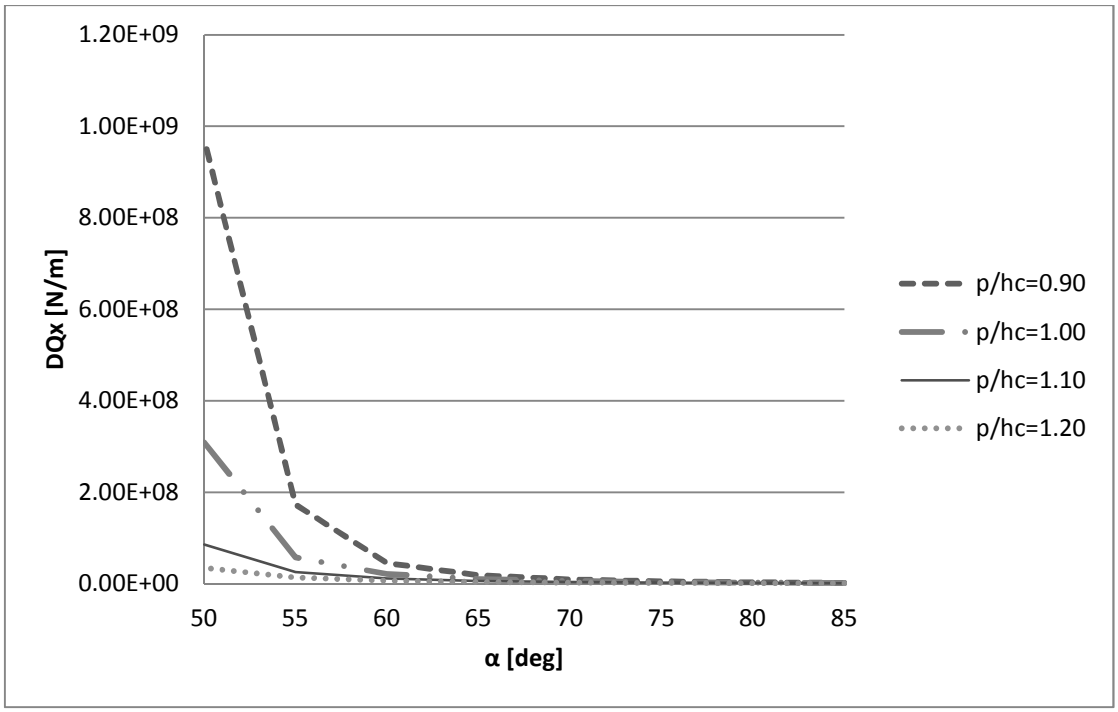


*Figure 1- 34 Shear stiffness $D_{Qx}$*

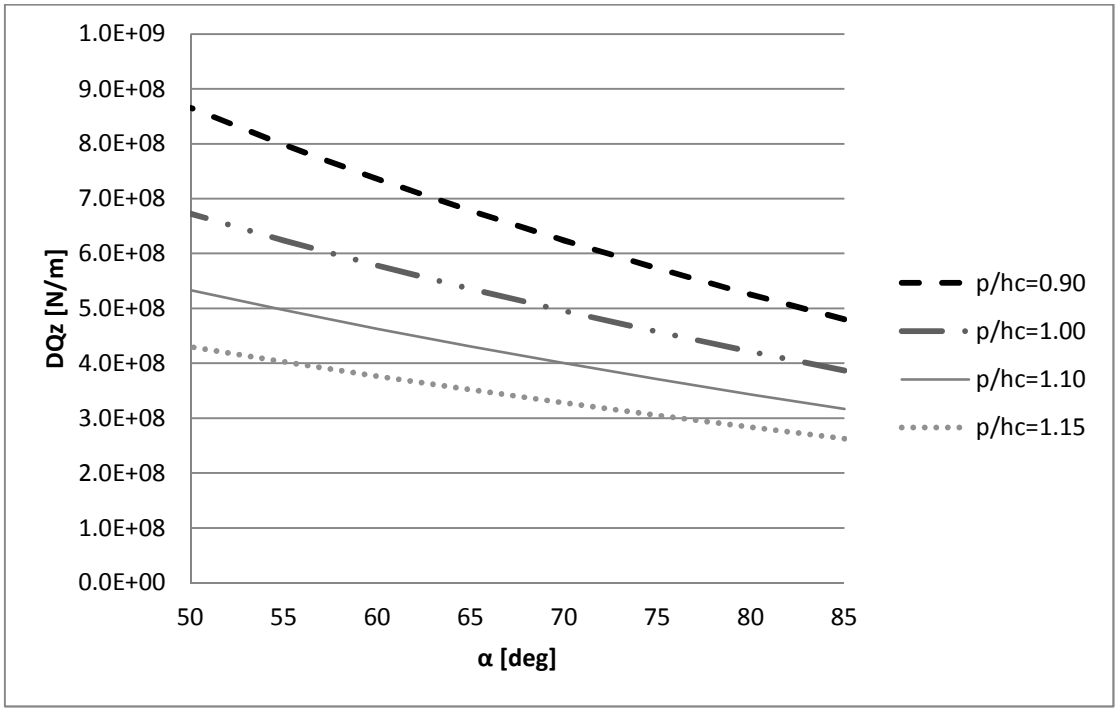


*Figure 1- 35 Shear stiffness $D_{Qz}$ in the direction of corrugation*

# 5 Bridge FE analysis

## 5.1 Introduction

In this chapter two concepts of a bridge deck are analysed. The different concepts are presented in Figure 1- 36. Concept I consists of an I-beam girder, and a complete steel sandwich panel (SPS) deck. In Concept II the upper flange of the I-beam, and the bottom plate of the SPS deck are omitted. The structural behaviour of the bridge was studied by conducting finite element analysis in Abaqus/CAE. Global and local deflection, stresses, buckling and fatigue strength were analysed.

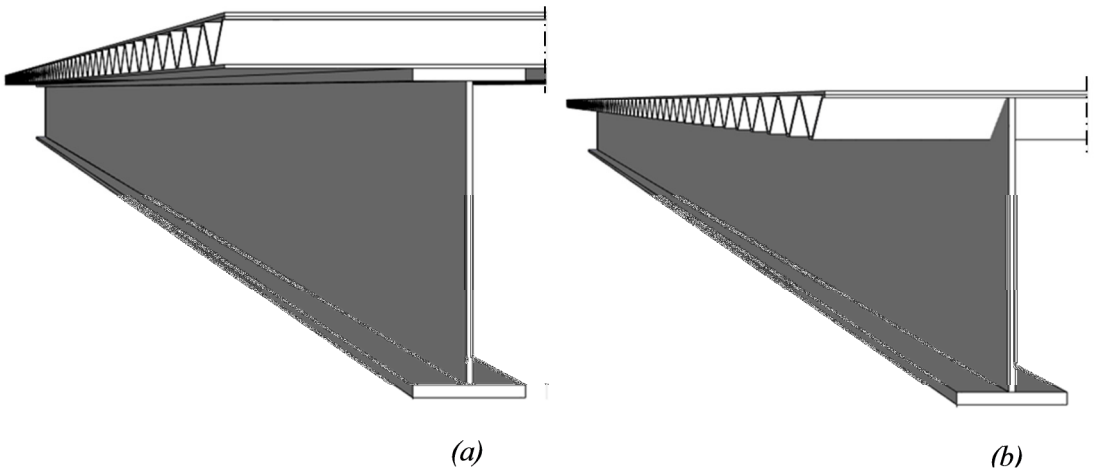


*Figure 1- 36 (a) Concept I, (b) Concept II*

## 5.2 Applied loads

### 5.2.1 Vertical loads

The bridge concepts were analysed for bridge loads according to Eurocode 1: Actions on structures – Part 2: Traffic loads on bridges (EN 1991-2: 2003). Load Model 1 (LM1) was used that consists of two load systems: double-axle concentrated loads, and uniformly distributed loads. The characteristic values were taken according to Table 1- 5. Dimensions of the bridge and the applied loads are presented in Figure 1-37. The bridge has 2 lanes, and according to Eurocode each lane is 3 m wide, with a remaining area of 1 m. For both load systems adjustment factors $\alpha_Q$ and $\alpha_q$ have to be considered. According to the National Annex the factors are 0.9 and 0.7, respectively for Lane 1, and for Lane 2 the values are 0.9 and 1, respectively.

*Table 1- 5 Load model (32)*

| **Location** | **Tandem system** | **UDL system** |
|---|---|---|
| | **Axle loads $Q_{ik}$ [kN]** | **$q_{ik}$ [kN/m$^2$]** |
| Lane number 1 | 300 | 9 |
| Lane number 2 | 200 | 2.5 |
| Remaining area | 0 | 2.5 |

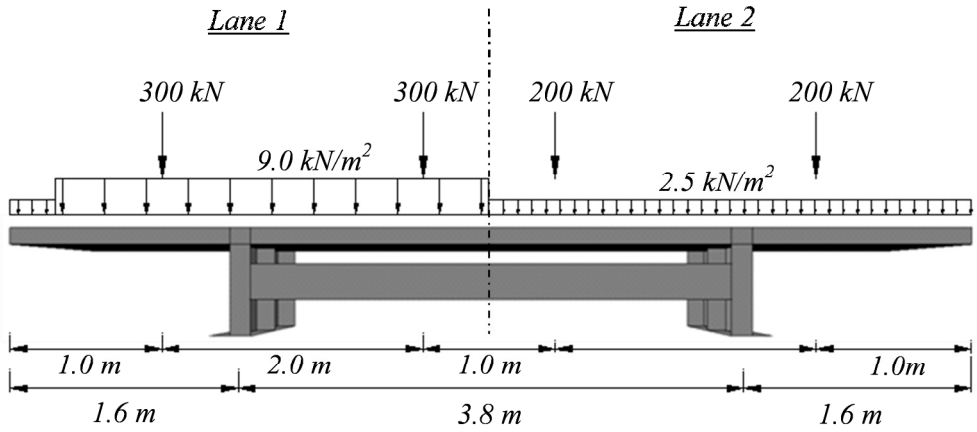


*Figure 1- 37 Load Model 1*

### 5.2.2 Horizontal loads

Horizontal forces that were considered in the analyses are the breaking and acceleration forces, and lateral forces. A braking force $Q_{lk}$ is acting on the surface of one lane, and is calculated as follows (32):

$$Q_{lk} = 0{,}6\alpha_{Q1}(2Q_{1k}) + 0{,}10\alpha_{q1}q_{1k}w_1L \tag{13}$$

The acceleration force is of the same magnitude as braking forces, but in the opposite direction. Lateral forces are equal to 25% of the longitudinal breaking or acceleration force $Q_{lk}$. For load calculations refer to APPENDIX C.

### 5.2.3 Fatigue loads

In fatigue analyses Load Model 3 (32) was applied on the bridge. This model consists of four axles, the weight of each axle is equal to 120 kN. General model for the wheel position and the wheel contact areas is presented in Figure 1- 38, where $w_1$ is lane width.

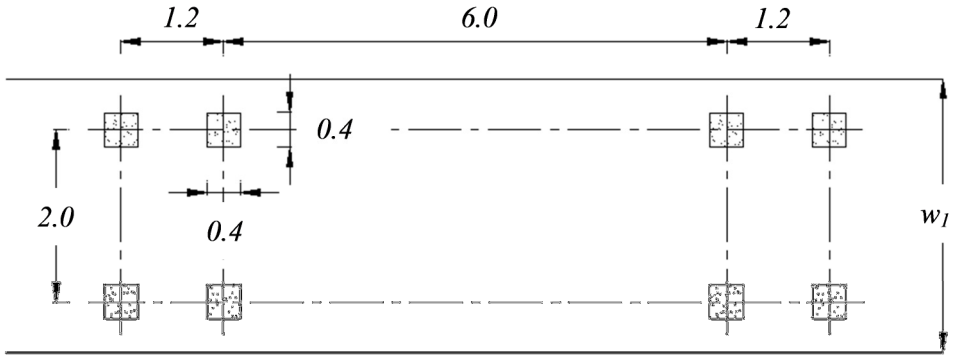


*Figure 1- 38 Fatigue Load Model 3 (unit: m) (1)*

## 5.3 Bridge dimensions

### 5.3.1 Concept I

The bridge dimensions including the length, width and the girders were chosen from an existing bridge in Northern Sweden. Accordingly, bridge length is 12 m, and it consists of two I-girders with the dimensions presented in Figure 1- 39. The bridge has two lanes, both 3.5 meters wide. To add lateral and torsional stability, the bridge is provided with three transversal beams HEA300.

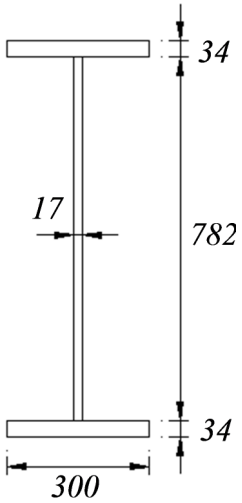


*Figure 1- 39 Steel girder dimensions (unit: mm)*

The deck of the bridge is a laser-welded steel sandwich panel. To start with the analysis initial parameters for the deck had to be determined. The initial design of core configuration shown in Figure 1- 40 (a) was chosen according to the parametric study presented in Chapter 3. In this study it was observed that the best structural performance of a steel sandwich panel is attained with a truss-like core configuration having an angle between 50 and 60 degrees. Due to manufacturing limitations a minimum horizontal part for welding had to be considered, and was initially chosen to be 27 mm. However, after static analyses the results showed very high local bending stresses under concentrate wheel load in the top plate, therefore the core parameters had to be changed. The only possibility to decrease length of the corrugation pitch, and at the same time to keep the angle between 50 and 60 degrees, was to lower the overall height of the deck. New dimensions for the core are presented in Figure 1- 40

(b). For a more detailed discussion about the effect of local bending stresses refer to Chapter 5.4.3.

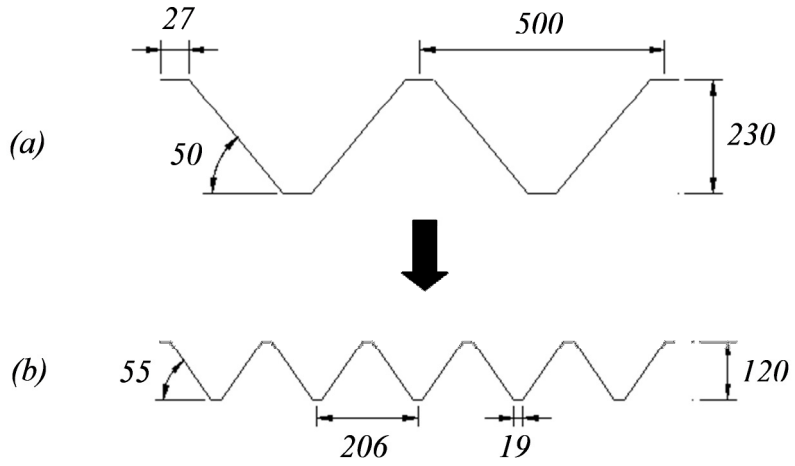


*Figure 1- 40 (a) initial core design for Concept I, (b) final core design for Concept I (unit: mm)*

Also, starting values for the deck thicknesses had to be chosen. According to common practice, the minimum required thickness for plates should be 8 mm. The thickness of the core was determined according to the elastic critical plate buckling stress equation for equivalent orthotropic plates, see Equation (14) that was obtained from EN 1993-1-1: 2005 (33). The critical stress $\sigma_{cr}$ was taken as 355 MPa, which is the yielding stress chosen for the steel in this bridge; for detailed calculations refer to APPENDIX C. Calculations resulted in the core thickness 3.17 mm, but it was decided to use 4 mm as the starting value.

$$t_{core} = \frac{\sigma_{cr} 12(1-\upsilon^2) b_{core}{}^2}{k\pi^2 E} \tag{14}$$

## 5.3.2 Concept II

From the obtained results for Concept I it was obvious that the main stress concentration, yielding and buckling occur either in the top plate or the core. Consequently, it was decided to improve the design of Concept I by omitting the bottom plate. This not only reduces the amount of steel in the deck, but also decreases the amount of welding, thus the concept should be more economical. The core configuration was the same as for Concept I, and the I-girder is of same height but with a shape presented in Figure 1- 41.

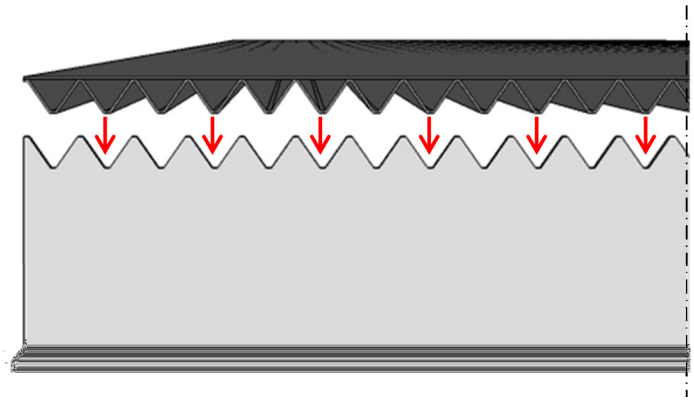

*Figure 1- 41 Concept II – assembly of the I-girder and the core*

## 5.4 Bending stresses

### 5.4.1 Global bending stresses

Global bending stresses were obtained in the mid-span of the bridge, where is the maximum bending moment. The tensile stresses were taken in the bottom flange of the girder, and the compressive stresses in the upper plate of the deck (see Figure 1- 42).

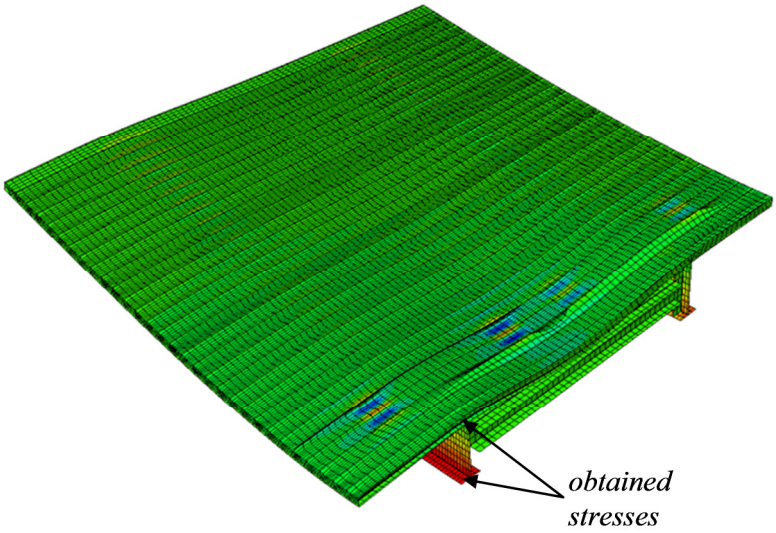


*Figure 1- 42 Bending stresses in the girder and the deck*

The bending behaviour and the stress distribution of the deck for both concepts is presented in Figure 1- 43 and in Figure 1- 44. The tensile stress in the mid-span of the bridge for Concept I is 283 MPa, and compressive stress -90 MPa. The neutral axis for Concept I is situated at a distance of 681 mm from the bottom flange of the girder, whereas Concept II has a downward shift in neutral axis, resulting in 555 mm. This is due to a decrease in the amount of material, and therefore an increase in stresses. Tensile and compressive stresses for Concept II are 319 MPa and -123 MPa, respectively. From the obtained stress distribution, it can be also concluded that composite action between the girder and the deck is achieved.

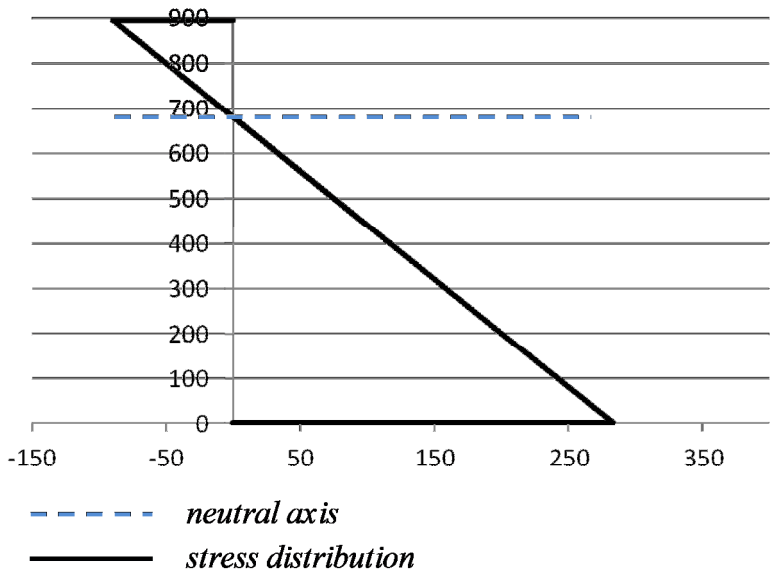


*Figure 1- 43 Concept I – stress distribution in the mid-span of the bridge, and the position of neutral axis*

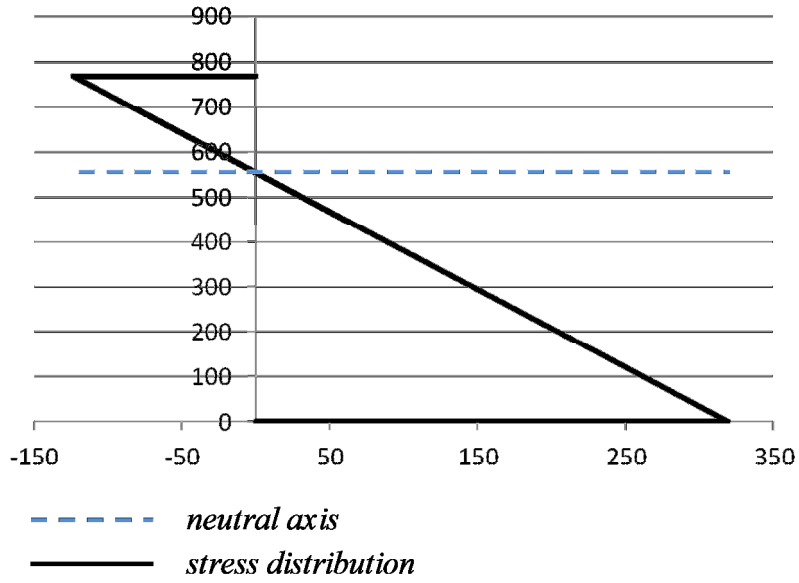


*Figure 1- 44 Concept II – stress distribution in the mid-span of the bridge, and the position of neutral axis*

### 5.4.2 Effective width

The effective deck width for both bridge concepts was calculated to account for shear lag in the deck. First, neutral axis was obtained from finite element analyses, and then effective width was computed from the equation of first moment of inertia. Core of the panel was omitted from calculations, and only the top plates were considered. Obtained effective widths are 2145 mm for Concept I, and 3020 mm for Concept II. Full material utilisation is achieved, when the whole deck is working compositely. It is the distance between girders divided by two, and plus the overhand, which in total is 3500 mm for one girder. For these two cases, 61% and 86% of the deck is working,

which are very good results. Especially in Concept II the deck is utilised in a very good way. Detailed calculations and derivations are presented in APPENDIX C.

### 5.4.3 Local bending stresses

Bending stresses were obtained in the Ultimate Limit State by applying Load Model 1. As mentioned previously, it was observed that very high local bending stresses caused by the wheel load are present in the deck for the initial core configuration in Concept I. As shown in Figure 1- 45 (a) the corrugation pitch $2p$ is equal to 500 mm, which is higher than the contact area of the wheel 400x400 mm. With a decreasing pitch length, as shown in Figure 1- 45 (b), an additional support for the wheel contact area is created – this reduces local bending stresses significantly, from initial bending stress 470 MPa to 323 MPa in the final core configuration (see Figure 1- 46).

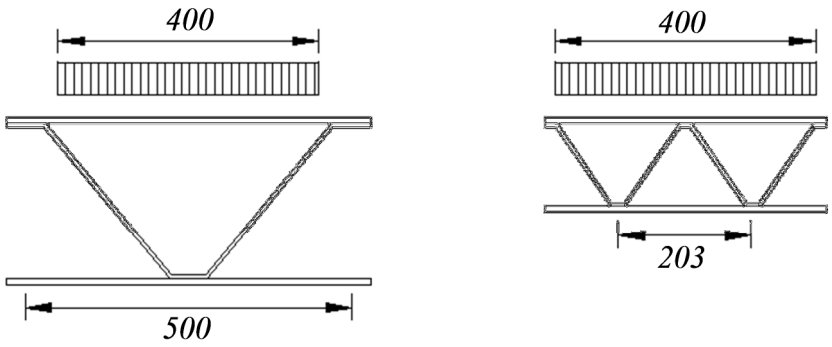


*Figure 1- 45 (a) first core configuration, (b) second core configuration*

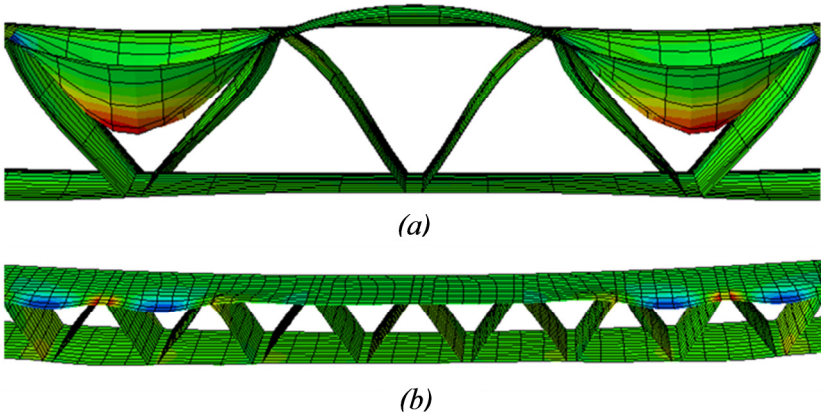


*Figure 1- 46 Local bending stresses for (a) initial core configuration, (b) final core configuration for Concept I*

Concept II (see Figure 1- 47) with the final chosen thicknesses, where core is 8 mm and top plate is 9 mm, has very high local bending stresses in the top plate (400 MPa). One possibility is to increase the core thickness to 9 mm, and the plate thickness to 10 mm. Consequently, bending stress would decrease down to 304 MPa. However, in this case increase in steel material would be 8%. A more economical solution would be to keep the initial thicknesses, and to add extra material to the areas with high stresses in the mid-span of the bridge.

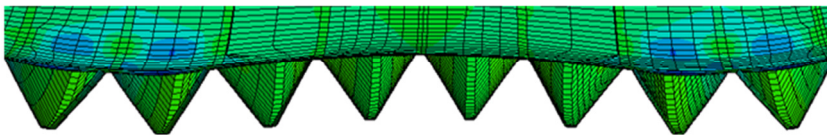

*Figure 1- 47 Local bending stresses for Concept II*

After local bending analyses it was observed that for Concept I the yielding takes place in the top plate under the wheel load. However, for Concept II, yielding in the connection of the core and the girder was detected. As seen in Figure 1- 48, there is very high load concentration along the girder, which is due to the transfer of forces. This phenomenon is not observed for Concept I. A close-up of the connection is represented in Figure 1- 49 for deck with a core and plate thickness 5 mm and 10 mm, respectively. Due to the yielding, flange and core thicknesses had to be changed. When increasing flange thickness 16% the effect on the yielding stress is very small, it decreases only 2.8%. When increasing core thickness 16%, yielding stress is decreasing 11.3% (see Table 1- 6). Thus, it is more reasonable to change the thickness of the core in order to obtain satisfactory stresses between connections.

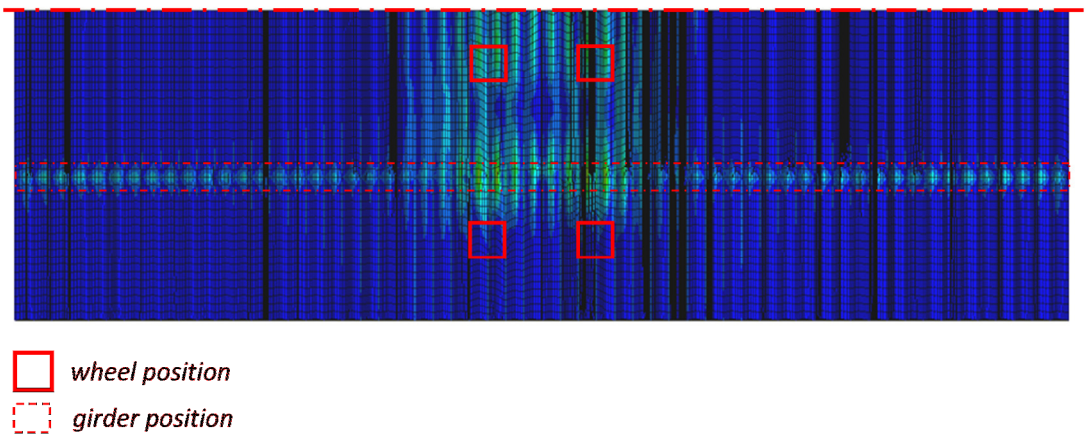


*Figure 1- 48 Concept II –high stress concentration in the connection between core and girder*

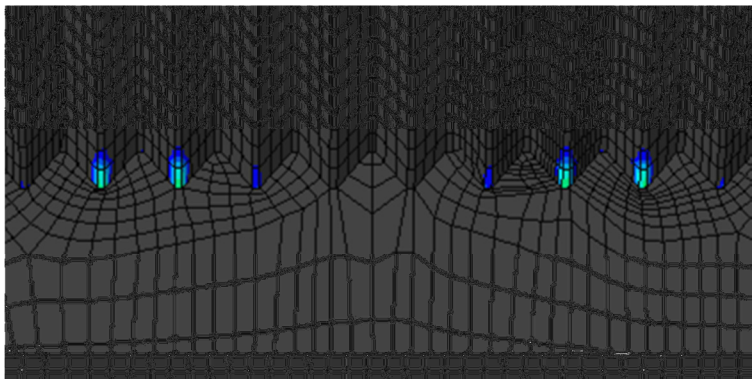

*Figure 1- 49 Concept II – Yielding at stress 355 MPa in the connection between girder and the core*

*Table 1- 6 Yielding stress for various core and flange thicknesses (Concept II)*

| **Yielding stress** | **Core thickness $t_c$ [mm]** | **Plate thickness $t_f$ [mm]** |
|---|---|---|
| 530 | 5 | 10 |
| 515 | 5 | 12 |
| 470 | 6 | 10 |
| 415 | 7 | 9 |
| 350 | 8 | 9 |

### 5.4.4 Shear stress

Maximum shear stresses between the girder and the deck are studied. The bridge is subjected to breaking and lateral load as shown in Figure 1- 50. In Abaqus/CAE it is not possible to create a line load for shell elements, therefore horizontal forces were applied as distributed traction forces on the area of 40x3000 mm. Shear stresses caused from breaking load are negligible and are much below the allowable limit $\frac{f_y}{\sqrt{3}} = 205\,MPa$, see Table 1- 7. As lateral load is 25% of the breaking load, shear stresses caused by lateral forces are even smaller, and therefore the values are not presented here.

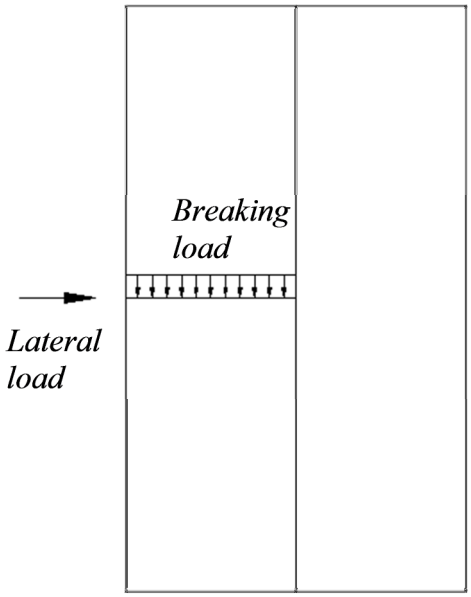


*Figure 1- 50 Breaking and lateral loads*

*Table 1- 7 Shear stresses from breaking load*

| Concept | Connection [MPa] | Deck [MPa] |
|---|---|---|
| I | 1.6 | 9.2 |
| II | 7.6 | 6.1 |

## 5.5 Buckling analysis

### 5.5.1 Vertical loads

Linear buckling analyses were conducted to determine the critical buckling modes and load factor $\lambda$ referred to as eigenvalue.

The first buckle could be observed in the deck; the eigenvalue obtained from the finite element analyses is 4.33 for Concept I and 3.68 for Concept II. It can be observed that there is a slight difference in buckling load factors between both concepts – Concept I has a higher value, and therefore is stiffer. Nevertheless, the obtained buckling factors have very high values, which refer to very high stiffness of the bridge elements.

For a detailed buckling assessment geometrical nonlinear analyses should also be carried out, where geometrical imperfections of the structure and nonlinear behaviour of the material are taken into account. However, the two bridge concepts presented in this thesis had no buckling problems in the linear analyses stage, and the buckling load factors were much above 1. Therefore, the nonlinearity was not accounted for in this thesis.

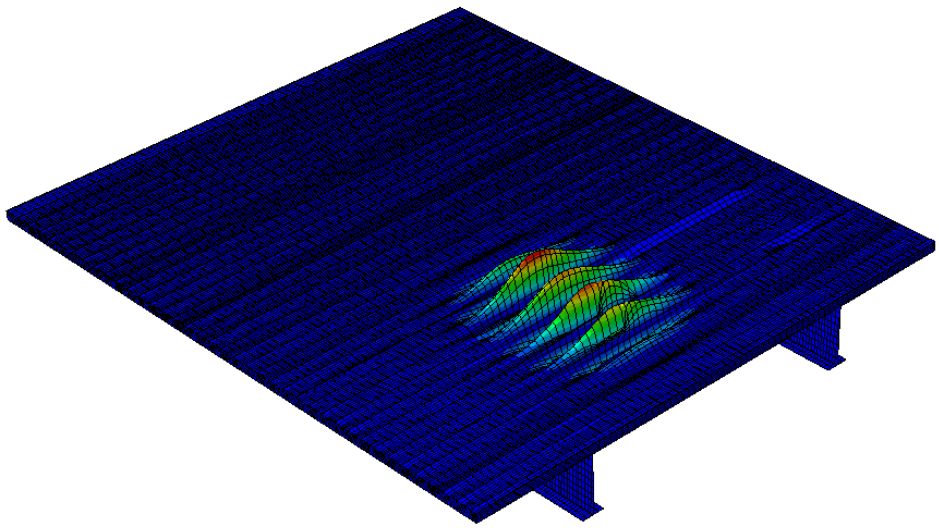

*Figure 1- 51 Concept I – second buckle in the deck*

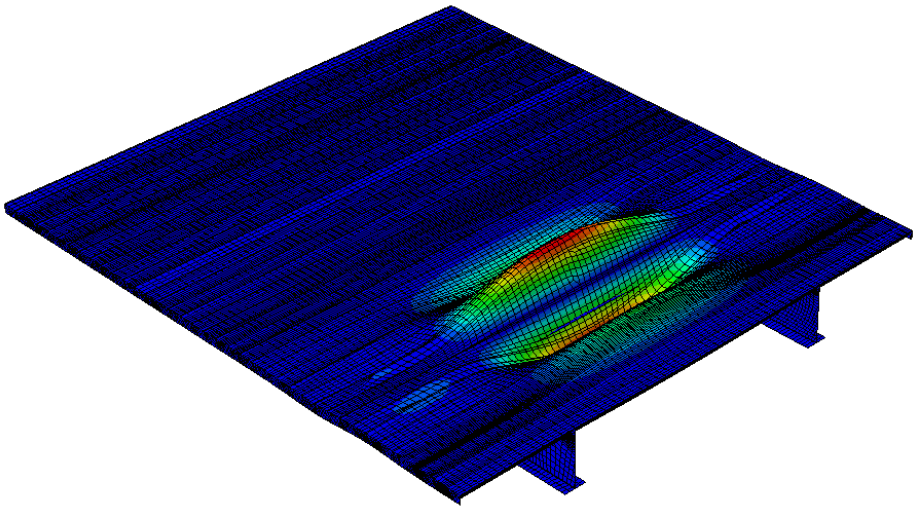

*Figure 1- 52 Concept II – second buckle in the deck*

### 5.5.2 Horizontal loads

The buckling factors that occur when applying breaking load on the structure were considered in the thesis as well. The first buckling mode appears in the deck; eigenvalue for Concept I and Concept II is 53.7 and 51.0, respectively. It can be concluded that when applying horizontal loads on the structure, no buckling risk is present. Representation of buckling shapes is shown in Figure 1- 53 and Figure 1- 54**.**

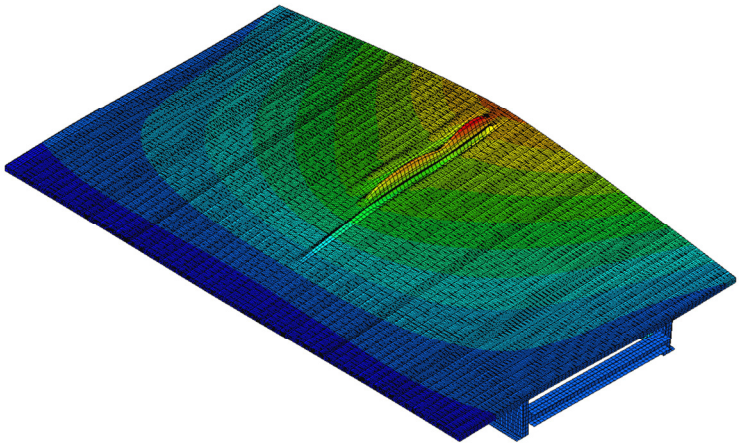

*Figure 1- 53 Concept I – buckling from braking load*

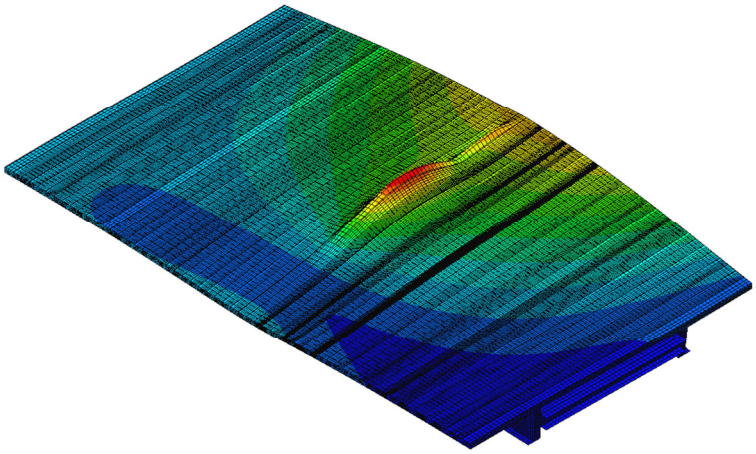

*Figure 1- 54 Concept II – buckling from braking load*

## 5.6 Fatigue strength

Fatigue assessment was carried out by applying Load Model 3 according to EN 1993-1-9. To find the load position for a maximum moment several cases were considered. The results showed that the maximum moment is obtained when concentrated loads are placed as shown in Figure 1- 55.

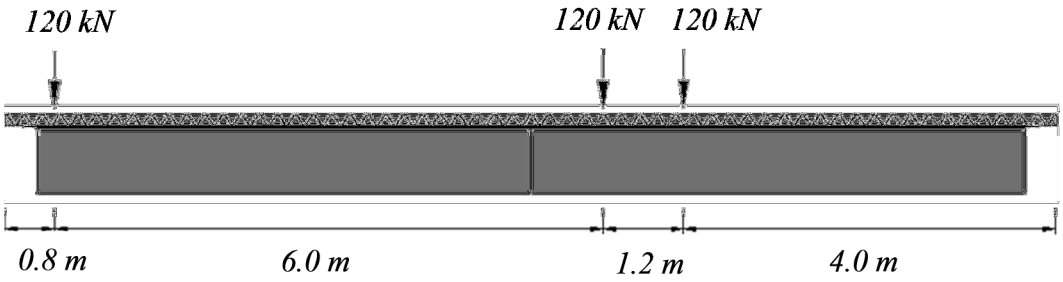


*Figure 1- 55 Wheel load positions causing maximum moment in the girder*

In this thesis the emphasis is on Concept II, where the girder is directly connected to the core using butt weld. In Eurocode there is no detail category for such connections, and therefore no fatigue strength for nominal stress range is given. The purpose was to give an indication of stresses by evaluating the magnitude of maximum in-plane stresses. Maximum stress in the connection is 54 MPa, as shown in Figure 1- 56; it is a reasonable stress if compared to existing detail categories presented in Eurocode, for instance detail 71 for toe cracking.

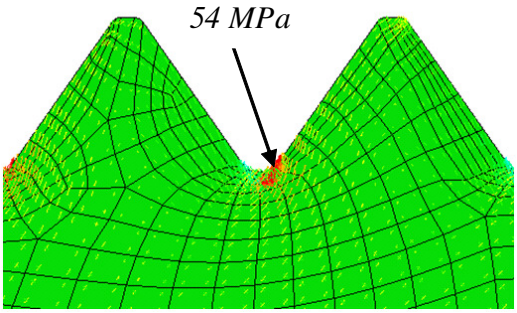


*Figure 1- 56 Obtained max stress in the connection*

## 5.7 Deflection in SLS

Assessment of the bridge deflection in serviceability limit state is made. Graphical representation of deflections for both bridge concepts is depicted in Figure 1- 57 and Figure 1- 58. Maximum deflection in the girder and in the deck is obtained in the mid-span of the bridge, and the values are presented in Table 1- 8. Deflection for Concept I is lower than for Concept II, this is due to the additional flange and bottom plate thickness. However, the deflection criterion $\frac{L}{400}$ is satisfied in both cases.

*Table 1- 8 Results for deflection for Concept I and Concept II*

| **Concept** | **Deflection in the girder [mm]** | **Deflection in the deck [mm]** |
|---|---|---|
| I | 19.1 | 0.5 |
| II | 28.0 | 4 |

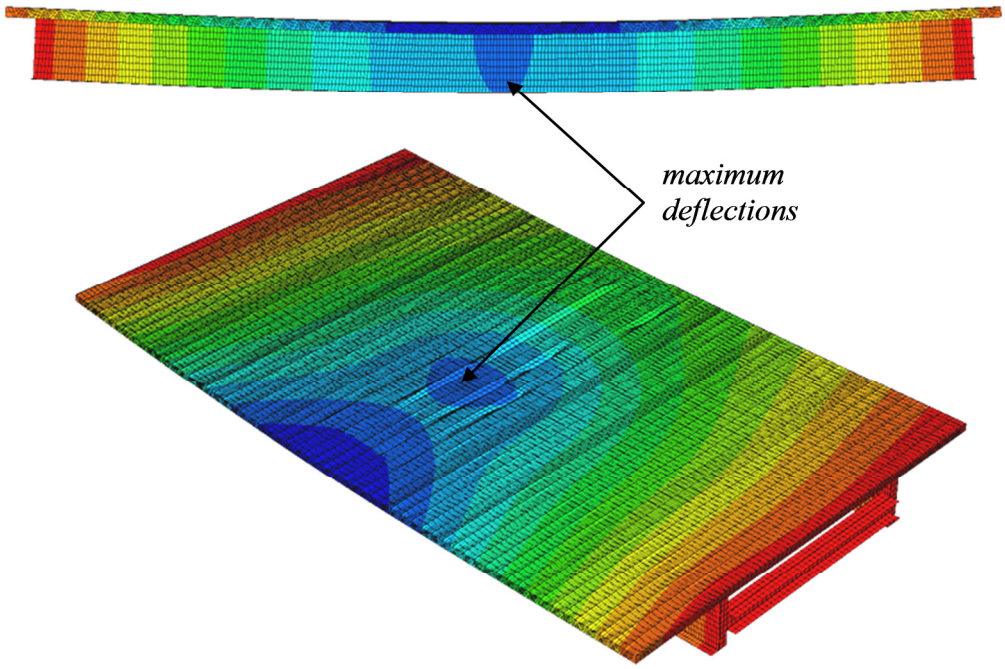


*Figure 1- 57 Concept I – maximum deflection in the deck and in the girder*

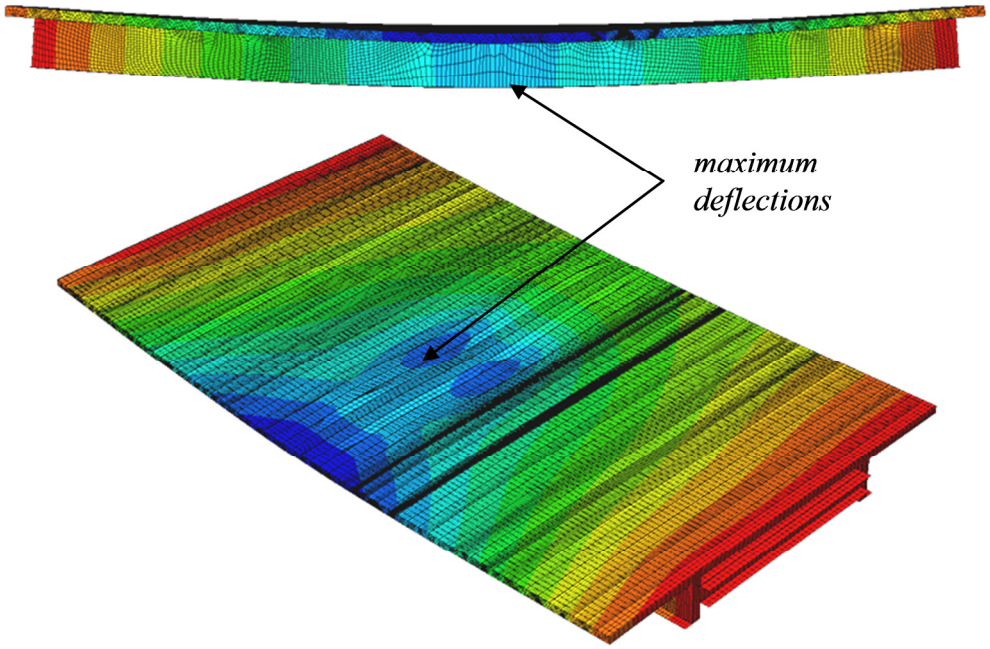


*Figure 1- 58 Concept II – maximum deflection in the deck and in the girder*

# 6 Conclusions and future research

## 6.1 Conclusions

In this work, a conceptual design of a possible steel sandwich bridge deck was established. Two bridge concepts were studied and geometric parameters for steel sandwich panels were chosen, which would satisfy structural requirements according to Eurocode.

From this thesis it was concluded, that:

- When choosing core configuration the flat segment of corrugation, angle, and pitch to core height ratio are important geometric parameters to consider.
- The study indicated that a sandwich plate with V-core performs better compared to other studied core types.
- In the bridge design, local bending stresses under concentrated wheel loads govern the design of the deck. Further optimization of the core shape and dimensions might lead to a more efficient and economic design.
- Two deck concepts with the same core configuration and dimensions were thoroughly studied. In the first concept the steel deck is composed of two (top and bottom) deck plates, while in Concept II, the bottom plate is omitted. Both deck concepts:
    - exhibit very stiff behaviour in bending,
    - have very low shear stresses,
    - have very good structural behaviour.
- Even though a thorough fatigue analysis was not performed, the values of stresses obtained from the FE-analysis are - for both deck concepts – so low, that fatigue should not govern the design of these decks.

## 6.2 Future research

In future research detailed analysis for the connections should be performed. Also, the production technology should be investigated and life-cycle cost analysis should be made to have an overview of the cost of this innovative deck in comparison to other decks.

The concept of sandwich steel decks in this thesis was only considered for simply-supported road bridges. Additional benefits may be obtained if the concept is used in other bridge types. In particular for continuous bridges, where cracking of concrete decks reduces their contribution to the structural system, sandwich steel decks should provide a valuable alternative.

Another bridge type for which the economic and structural feasibility of sandwich steel decks should be considered is movable bridges. Conventional orthotropic bridge decks have until now been used in this kind of bridges where weight reduction brings many benefits.

Finally, it should be mentioned that the work in this thesis was meant as a path definer. Further, and more accurate analysis of various possible configurations and structural solutions should be studied in order to find optimized solutions for different bridge applications.

# 7 Bibliography


1. **Telford, T.** *Fourth International Conference on Current and Future Trends in Bridge Design, Construction and Maintenance.* 2006.

2. **Feldmann, M, Sedlacek, G and Ge ler, A.** *A system of steel-elastomer sandwich platesfor strengthening orthotropic bridge decks.* 2007.

3. **Intelligent Engineering.** SPS The Sandwich Plate System. [Online] http://www.ie-sps.com.

4. **Martin, James David.** *Sandwich plate system bridge deck tests.* Virginia : s.n., 2005.

5. **Cousins, Thomas E., Murray, Thomas M and Harris, Devin K.** *Use of a sandwich plate plate system in a Virginia bridge.* Charlottesville, Virginia : s.n., 2009.

6. **Kennedy, Stephen J and Murray, Thomas M.** *Ultimate Strength of an SPS Bridge – The Shenley Bridge, Québec, Canada.* Québec City, Québec, Canada : s.n., 2004.

7. **Kennedy, Stephen J. and Kennedy, D. J. Laurie.** *SPS creates new markets for steel.*

8. **Säynäjäkangas, J and Taulavuori, T.** *A review in design and manufacturing of stainless steel sandwich panels.* s.l. : http://www.stainless-steel-world.net/, 2004.

9. *Design Implification of Sandwich Panels.* **Hoffart, J and Hansen, E.** 2008, Welding Magazine.

10. **Abbott, S.P., et al.** *Automated Laser Welded High Performance Steel Sandwich Bridge Deck Development.* 2007.

11. **Roland, F and Reinert, T.** *Laser welded sandwich panels for the shipbuilding industry.* 2000.

12. **Romanoff, J.** *Bending response of laser-welded web-core sandwich plates.* 2007.

13. **Kalnins, K and Eglitis, E.** *Metamodels for optimum design of laser welded sandwich structures.* 2008.

14. **Romanoff, J. and Varsta, P.** *Bending Response of Web-core Sandwich Beams.* 2006.

15. **Romanoff, J., Varsta, P. and Klanac, A.** *Stress Analysis of Homogenized Web-Core Sandwich Beams.* 2007.

16. **Romanoff, J., et al.** *The Stiffness of Laser Stake Welded T-joints in Web-core Sandwich Structures* . 2007.

17. **Romanoff, J. and Varsta, P.** *Bending response of web-core sandwich plates.* 2007.

18. **Romanoff, J, Varsta, P and Remes, H.** *Laser-welded web-core sandwich plates under patch loading.* 2007.

19. *Steel Sandwich Panels in Marine Applications.* **Kujala, P and Klanac, A.** 2005.

20. **Bright, S.R and Smith, J.W.** *A new design for steel bridge decks using laser fabrication.* 2007.

21. Advanced composite sandwich steel structures. [Online] 2000. http://sandwich.balport.com/public_downloads/public-project-summary.pdf.

22. **Denney, P.** Hybrid laser arc welding: Has its time arrived? [Online] 2011. http://www.industrial-lasers.com/articles/print/volume-26/issue-1/features/hybrid-laser-arc-welding-has-its-time-arrived.html.

23. **Miller, C.B.** U.S. Laser Corporation. [Online] 2011. http://www.uslasercorp.com/envoy/welding.html.

24. **Caccese, V and Yorulmaz, S.** *Laser Welded Steel Sandwich Panel Bridge Deck Development: Finite Element Analysis and Stake Weld Strength Tests.* 2009.

25. **Sarma, D.K, et al.** *Hybrid Laser Welding : Process Advantages and Application for Shipbuilding.*

26. **Libove, C and Hubka, Ralph E.** *Elastic constants for corrugated-core sandwich plates.* 1951.

27. **Chang, Wan-Shu, et al.** *Bending behaviour of corrugated-core sandwich plates.* 2005.

28. **Tan, K.H, Montague, P and Norris, C.** *Steel sandwich panels: finite element, closed solution, and experimental comparisons on a 6m x 2.1m panel.* 1989.

29. **Zangani, D, Robinson, M and Gibson, A.G.** *Evaluation of stiffness terms for Z-cored sandwich panels.* 2007.

30. **Lok, Tat-Seng and Cheng, Quin-Hua.** *Elastic stiffness properties and behaviour of truss-core sandwich panel.* 2000.

31. **Lok, T.S and Cheng, Q.H.** *Elastic Deflection of Thin-Walled Sandwich Panel.* 1999.

32. *Eurocode 1: Actions on structures - part 2: Traffic loads on bridges. EN 1991-2:2003.* s.l. : CEN, 2003.

33. *Eurocode 3: Design of steel structures – Part 1-1: General rules and rules for buildings.* s.l. : CEN, 2005.

34. **Romanoff, J., Varsta, P. and And Remes, H.** *Laser-Welded Web-Core Sandwich Plates under Patch-Loading.* 2007.

# APPENDIX A

## Calculation of elastic constants for a V-corrugation

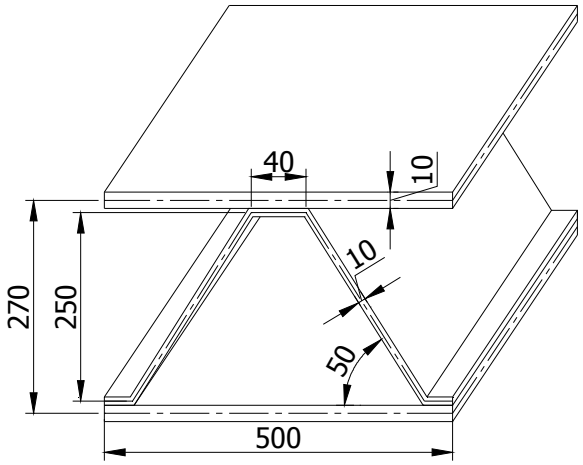


**Initial data:**

$\nu = 0.3$

$G = \frac{E}{2\cdot(1+\nu)} = 80769\cdot\frac{N}{mm^2}$

$t_f = 10mm$

$t_c = 10mm$

$h_c = 250mm$

$p = 250mm$

$\alpha = 50deg$

$f = p - \frac{h_c}{\tan(\alpha)} = 40.225\cdot mm$

$l_{width} = 2p = 500\cdot mm$

$a_{bottom} = p - \frac{f}{2} = 229.887\cdot mm$

$h = h_c + t_f + t_c = 270\cdot mm$

$x = \frac{h_c}{\tan(\alpha)} = 209.775\cdot mm$

$s = \frac{h_c}{\sin(\alpha)} = 326.352\cdot mm$

**Bending stiffness:**

$$I_f = 2\left[2 \cdot p \cdot t_f \cdot \left(\frac{h}{2}\right)^2\right] = 1.822 \times 10^{-4}\,m^4$$

$$I_c = 2 \cdot \left[f \cdot t_c \cdot \left(\frac{h_c}{2}\right)^2\right] + \frac{2 \cdot t_c \cdot s^3}{12} \cdot \sin(\alpha)^2 = 4.657 \times 10^{-5}\,m^4$$

$$EA_z = 2\left(E \cdot t_f\right) + E \cdot \frac{2 \cdot f \cdot t_c + 2 \cdot s \cdot t_c}{2p} = 7.279 \times 10^6 \cdot \frac{N}{mm}$$

$$D_{zz} = E \cdot \left(I_c + I_f\right) = 4.805 \times 10^7 \cdot N \cdot m^2$$

$$D_z = D_{zz} \cdot \frac{1}{2p} = 9.61 \times 10^7 \cdot N \cdot m$$

$$EA_x = 2 \cdot E \cdot t_f + \left(\frac{2f \cdot t_c}{2p} \cdot E\right) = 4.538 \times 10^6 \cdot \frac{N}{mm}$$

$$D_{xx} = \frac{E \cdot I_f}{1 - \nu^2\left(1 - \frac{E \cdot I_f}{D_{zz}}\right)} = 3.899 \times 10^7 \cdot N \cdot m^2$$

$$D_x = D_{xx} \cdot \frac{1}{2p} = 7.797 \times 10^7 \cdot N \cdot m$$

**Twisting stiffness:**

$$D_{xz} = 2 \cdot G \cdot I_f \cdot \frac{1}{2p} = 5.888 \times 10^7 \cdot N \cdot m$$

**Transverse shear stiffness in the direction of corrugations:**

$$l_c = s + f = 366.577 \cdot mm$$

$$A_{cc} = \frac{l_c \cdot t_c}{p} = 14.663 \cdot mm$$

$$D_{Qz} = \frac{G \cdot t_c \cdot h^2}{p \cdot l_c} = \frac{G \cdot t_c^{\,2}}{A_{cc}} \cdot \left(\frac{h}{p}\right)^2$$

$$D_{Qz} = \frac{G \cdot t_c \cdot h^2}{p \cdot l_c} = 6.425 \times 10^8 \cdot \frac{N}{m}$$

**Transverse shear stiffness:**

$k_x = 1 \quad k_y = 1 \quad R_{c1} = 0$

$a_1 = \frac{h_c}{2} = 125 \cdot mm$

$j_1 = a_1 = 125 \cdot mm$

$d_1 = \frac{s}{2} = 163.176 \cdot mm$

$$D_{Qx} = S \cdot h \cdot \left( \frac{E}{1 - \nu_c^{\,2}} \right) \cdot \left( \frac{t_c}{h_c} \right)^3$$

$$K_{Iy} = \frac{2}{3} \cdot \left( \frac{d_1 \cdot \cos(\alpha)}{h_c} \right)^2 \cdot \frac{d_1}{h_c} + \frac{2}{3} \left[ \frac{1}{8} \cdot \left( \frac{p}{h_c} \right)^3 - \left( \frac{d_1 \cdot \cos(\alpha)}{h_c} \right)^3 \right] = 0.111$$

$$K_{Ixy} = \frac{2}{3} \cdot \frac{j_1}{h_c} \cdot \frac{d_1 \cdot \cos(\alpha)}{h_c} \cdot \frac{d_1}{h_c} + \frac{1}{2} \left[ \frac{1}{4} \cdot \left( \frac{p}{h_c} \right)^2 - \left( \frac{d_1 \cdot \cos(\alpha)}{h_c} \right)^2 \right] = 0.128$$

$$K_{Ix} = \frac{2}{3} \cdot \left( \frac{j_1}{h_c} \right)^2 \cdot \frac{d_1}{h_c} + \frac{1}{4} \cdot \frac{f}{h_c} = 0.149$$

$$K_{Lx} = \frac{f}{h_c} + 2 \cdot \frac{d_1}{h_c} \cdot \cos(\alpha)^2 = 0.7$$

$$K_{Lxy} = 2 \cdot \frac{d_1}{h_c} \cdot \sin(\alpha) \cdot \cos(\alpha) = 0.643$$

$$K_{Ly} = 2 \cdot \frac{d_1}{h_c} \cdot \sin(\alpha)^2 = 0.766$$

$$B_1 = K_{Iy} + \frac{1}{12} \left( \frac{t_c}{h_c} \right)^2 \cdot K_{Ly} = 0.111$$

$$B_2 = K_{Ixy} - \frac{1}{12} \left( \frac{t_c}{h_c} \right)^2 \cdot K_{Lxy} = 0.128$$

$$B_3 = K_{Ix} + \frac{1}{12} \left( \frac{t_c}{h_c} \right)^2 \cdot K_{Lx} = 0.149$$

$$B_4 = \frac{1-\nu^2}{1-\nu^2}\cdot\left(\frac{t_f}{t_c}\right)^3 = 1$$

$$S = \frac{6\cdot\frac{h_c}{p}\cdot B_1\cdot B_4 + \left(\frac{p}{h_c}\right)^2}{12\left[-2\left(\frac{p}{h_c}\right)^2\cdot B_2 + \frac{h_c}{h}\left[6\cdot B_4\cdot\left(B_1\cdot B_3 - B_2^{\,2}\right) + \left(\frac{p}{h_c}\right)^3\cdot B_3\right] + \frac{h}{h_c}\cdot\frac{p}{h_c}\cdot B_1\right]} = 75.287$$

$$D_{Qx} = S\cdot h\cdot\left(\frac{E}{1-\nu^2}\right)\cdot\left(\frac{t_c}{h_c}\right)^3 = 3.002\times 10^8\cdot\frac{N}{m}$$

# APPENDIX B

## Results from optimization study

*Table 1- 9 Results from optimization study*

| $p/h_c$ | $h_c/t_c$ | $h_c$ [mm] | $t_f$ [mm] | $t_c$ [mm] | angle [deg] | $D_x$ [Nm] | $D_z$ [Nm] | $D_{xz}$ [N/m] | $D_{Qx}$ [N/m] | $D_{Qz}$ [N/m] |
|---|---|---|---|---|---|---|---|---|---|---|
| 0.90 | 30.7 | 260 | 10 | 8.5 | 85 | 8.4E+07 | 1.2E+08 | 6.3E+07 | 2.0E+06 | 4.8E+08 |
| | 29.4 | | | 8.9 | 80 | 8.4E+07 | 1.2E+08 | 6.3E+07 | 3.2E+06 | 5.3E+08 |
| | 28.2 | | | 9.2 | 75 | 8.4E+07 | 1.2E+08 | 6.3E+07 | 5.3E+06 | 5.7E+08 |
| | 27.1 | | | 9.6 | 70 | 8.4E+07 | 1.2E+08 | 6.3E+07 | 9.5E+06 | 6.2E+08 |
| | 26.0 | | | 10.0 | 65 | 8.4E+07 | 1.1E+08 | 6.3E+07 | 1.9E+07 | 6.8E+08 |
| | 25.0 | | | 10.4 | 60 | 8.5E+07 | 1.1E+08 | 6.4E+07 | 4.5E+07 | 7.4E+08 |
| | 24.0 | | | 10.8 | 55 | 8.5E+07 | 1.1E+08 | 6.4E+07 | 1.7E+08 | 8.0E+08 |
| | 23.1 | | | 11.3 | 50 | 8.5E+07 | 1.1E+08 | 6.4E+07 | 9.7E+08 | 8.7E+08 |
| 1.00 | 32.4 | 260 | 10 | 8.0 | 85 | 8.3E+07 | 1.2E+08 | 6.2E+07 | 1.4E+06 | 3.9E+08 |
| | 31.1 | | | 8.4 | 80 | 8.4E+07 | 1.2E+08 | 6.3E+07 | 2.2E+06 | 4.2E+08 |
| | 29.9 | | | 8.7 | 75 | 8.4E+07 | 1.1E+08 | 6.3E+07 | 3.5E+06 | 4.6E+08 |
| | 28.7 | | | 9.1 | 70 | 8.4E+07 | 1.1E+08 | 6.3E+07 | 5.7E+06 | 5.0E+08 |
| | 27.7 | | | 9.4 | 65 | 8.4E+07 | 1.1E+08 | 6.3E+07 | 1.0E+07 | 5.4E+08 |
| | 26.7 | | | 9.8 | 60 | 8.4E+07 | 1.1E+08 | 6.3E+07 | 2.1E+07 | 5.8E+08 |
| | 25.7 | | | 10.1 | 55 | 8.4E+07 | 1.1E+08 | 6.3E+07 | 5.8E+07 | 6.2E+08 |
| | 24.8 | | | 10.5 | 50 | 8.4E+07 | 1.0E+08 | 6.4E+07 | 3.1E+08 | 6.7E+08 |
| 1.10 | 34.1 | 260 | 10 | 7.6 | 85 | 8.3E+07 | 1.1E+08 | 6.2E+07 | 1.1E+06 | 3.2E+08 |
| | 32.8 | | | 7.9 | 80 | 8.3E+07 | 1.1E+08 | 6.2E+07 | 1.6E+06 | 3.4E+08 |
| | 31.6 | | | 8.2 | 75 | 8.3E+07 | 1.1E+08 | 6.3E+07 | 2.4E+06 | 3.7E+08 |
| | 30.4 | | | 8.6 | 70 | 8.3E+07 | 1.1E+08 | 6.3E+07 | 3.7E+06 | 4.0E+08 |
| | 29.3 | | | 8.9 | 65 | 8.4E+07 | 1.1E+08 | 6.3E+07 | 6.2E+06 | 4.3E+08 |
| | 28.4 | | | 9.2 | 60 | 8.4E+07 | 1.1E+08 | 6.3E+07 | 1.1E+07 | 4.6E+08 |
| | 27.4 | | | 9.5 | 55 | 8.4E+07 | 1.1E+08 | 6.3E+07 | 2.6E+07 | 5.0E+08 |
| | 26.5 | | | 9.8 | 50 | 8.4E+07 | 1.0E+08 | 6.3E+07 | 8.6E+07 | 5.3E+08 |
| 1.20 | 35.8 | 260 | 10 | 7.3 | 85 | 8.3E+07 | 1.1E+08 | 6.2E+07 | 7.9E+05 | 2.6E+08 |
| | 34.5 | | | 7.5 | 80 | 8.3E+07 | 1.1E+08 | 6.2E+07 | 1.1E+06 | 2.8E+08 |
| | 33.2 | | | 7.8 | 75 | 8.3E+07 | 1.1E+08 | 6.2E+07 | 1.7E+06 | 3.1E+08 |
| | 32.1 | | | 8.1 | 70 | 8.3E+07 | 1.1E+08 | 6.2E+07 | 2.5E+06 | 3.3E+08 |
| | 31.1 | | | 8.4 | 65 | 8.3E+07 | 1.1E+08 | 6.3E+07 | 4.0E+06 | 3.5E+08 |
| | 30.0 | | | 8.7 | 60 | 8.3E+07 | 1.1E+08 | 6.3E+07 | 6.8E+06 | 3.8E+08 |
| | 29.1 | | | 8.9 | 55 | 8.3E+07 | 1.1E+08 | 6.3E+07 | 1.3E+07 | 4.0E+08 |
| | 28.2 | | | 9.2 | 50 | 8.3E+07 | 1.0E+08 | 6.3E+07 | 3.4E+07 | 4.3E+08 |

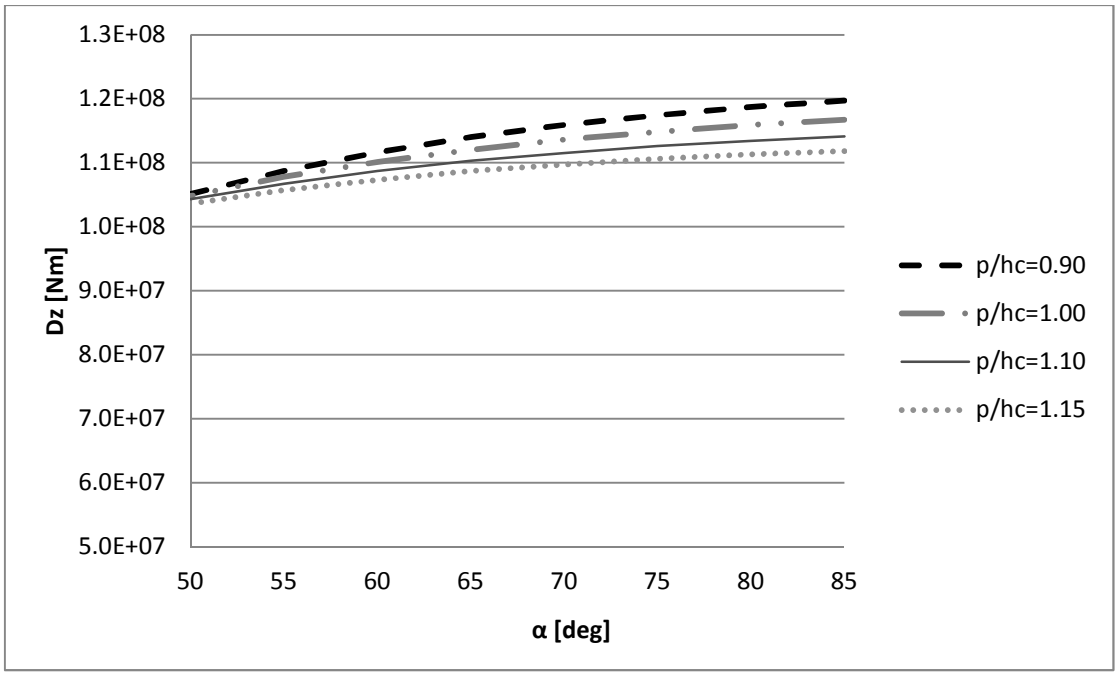


*Figure 1- 59 Bending stiffness Dz*

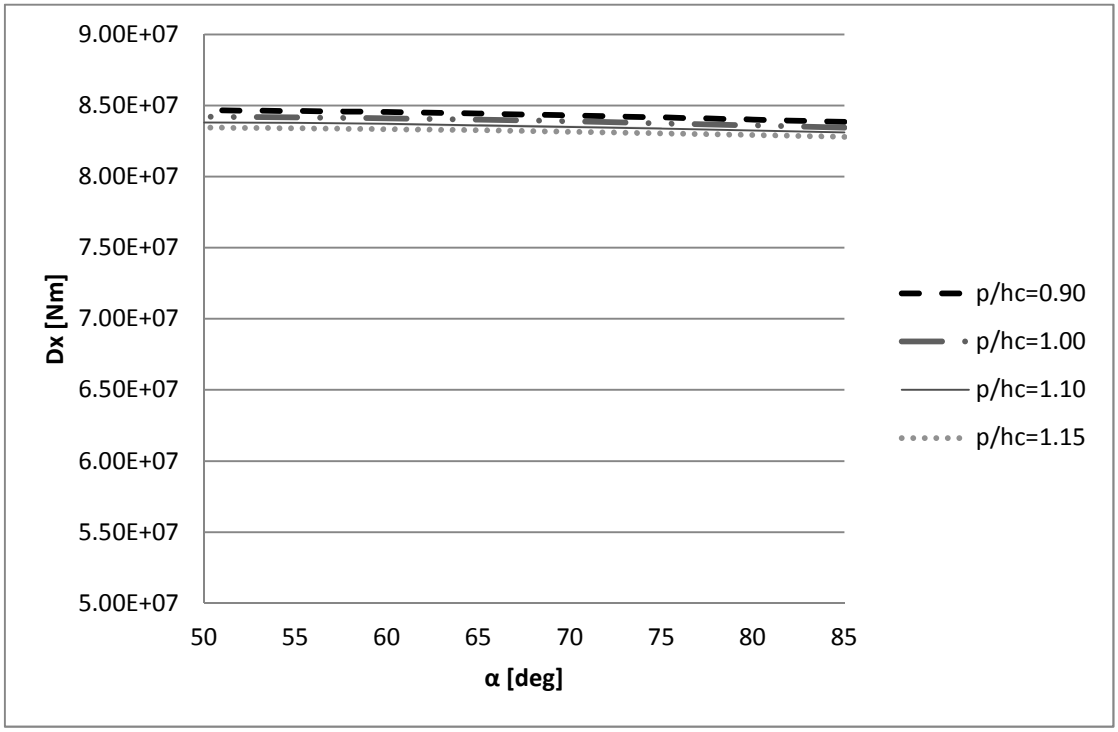


*Figure 1- 60 Bending stiffness Dx*

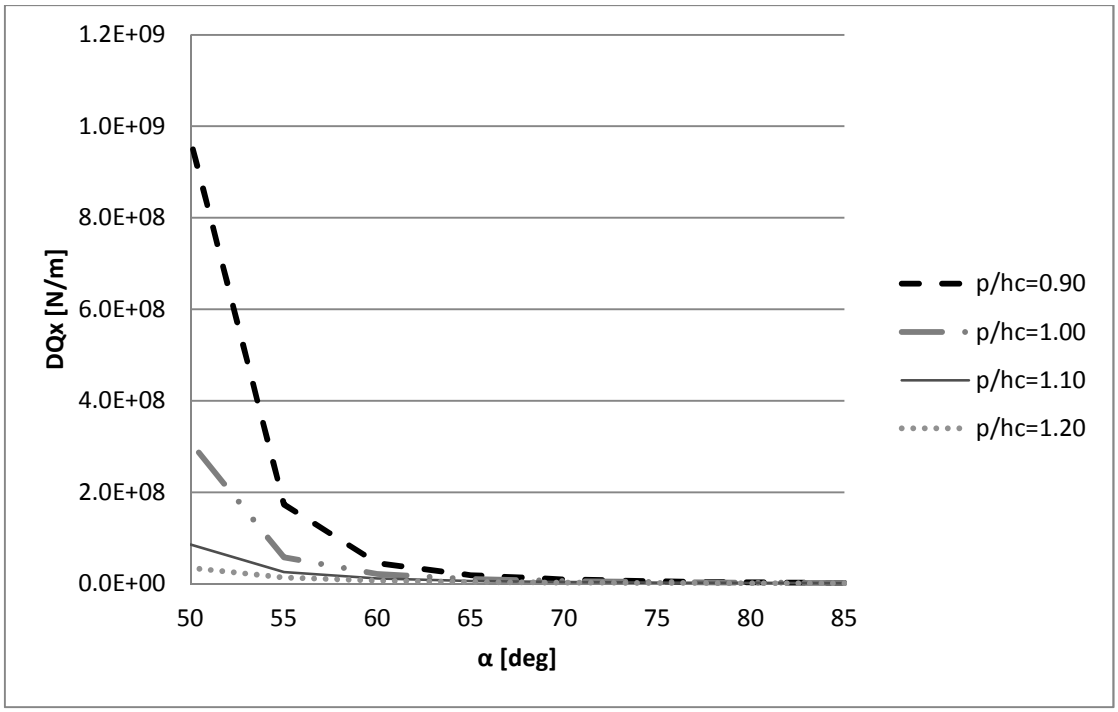


*Figure 1- 61 Shear stiffness $D_{Qx}$*

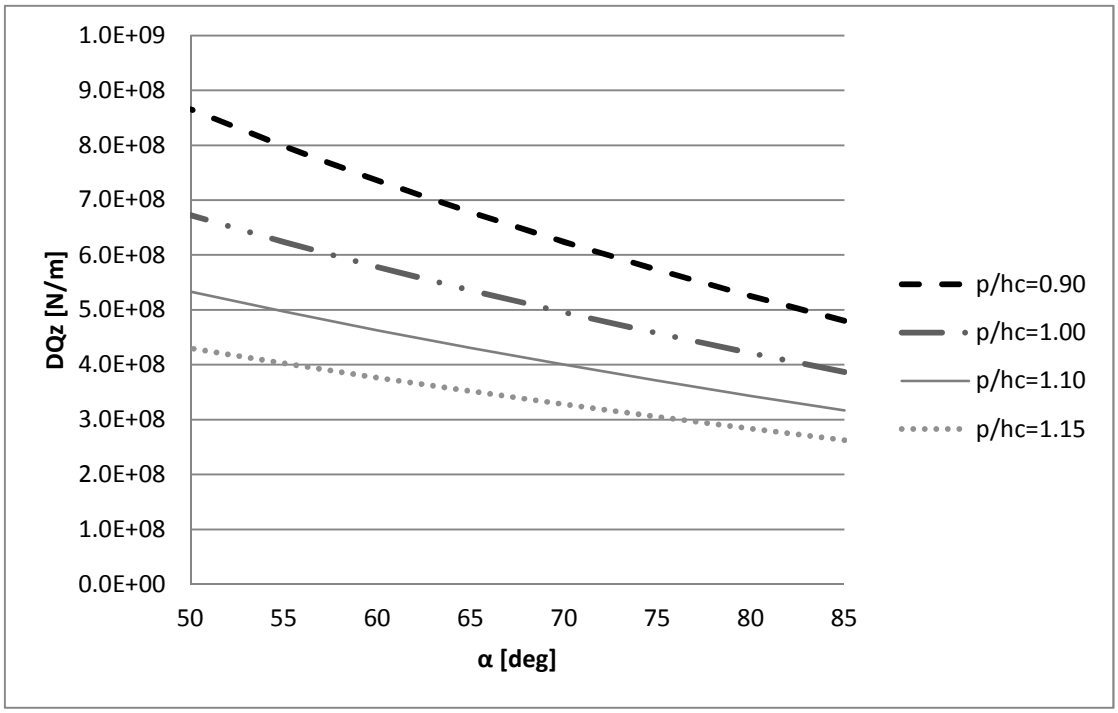


*Figure 1- 62 Shear stiffness $D_{Qz}$*

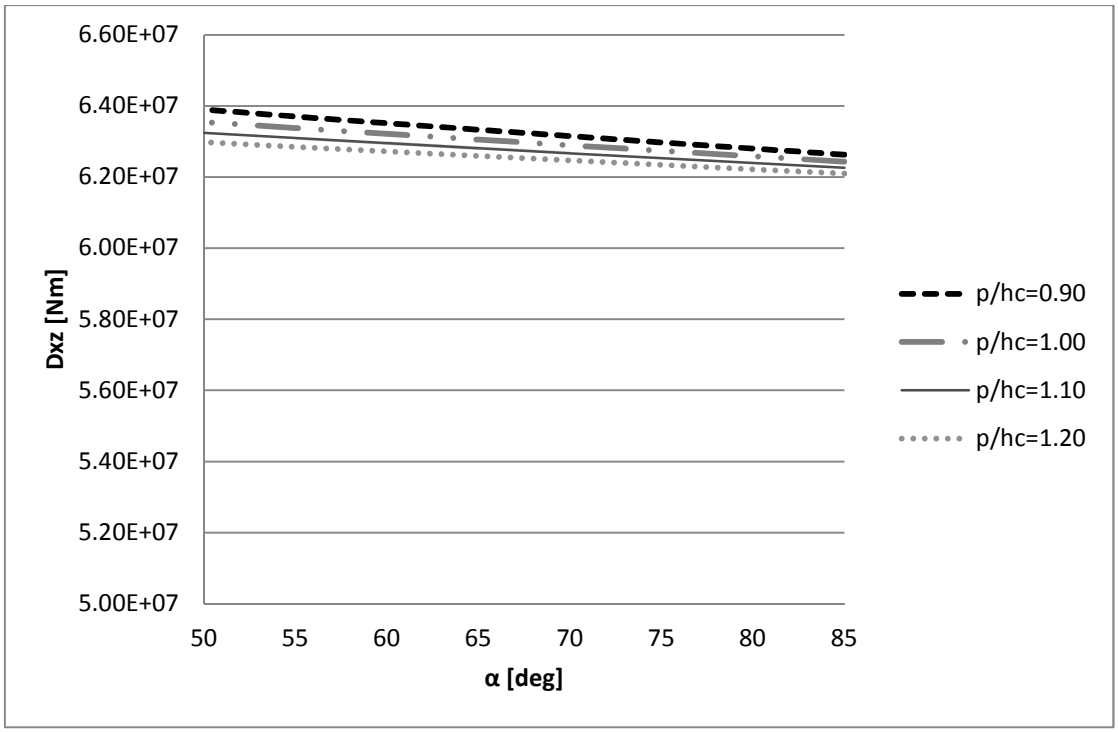


*Figure 1- 63 Twisting stiffness Dxz*

# APPENDIX C
## Bridge FE calculations

**Determination of minimum core thickness**

Elastic critical plate buckling stress of a plate:

$$\sigma_{cr} = \frac{\pi^2 \cdot E \cdot t^2}{12 \cdot \left(1 - \nu^2\right) \cdot b^2}$$

Critical stress is set equal to the yielding stress $f_y$, which is 355 MPa.

$$\sigma_{cr} = \frac{\pi^2 \cdot E \cdot t^2}{12 \cdot \left(1 - \nu^2\right) \cdot b^2}$$

$$f_{yd} = 355\text{MPa}$$

$$\sigma_{cr} = f_{yd} = 355 \cdot \text{MPa}$$

$$k = 4$$

$$\nu = 0.3$$

$$b_c = 146.49\text{mm}$$

$$E = 210\text{GPa}$$

$$t_c = \left[\frac{\sigma_{cr} \cdot 12 \cdot \left(1 - \nu^2\right) \cdot b_c^2}{k \cdot \pi^2 \cdot E}\right]^{0.5} = 3.168 \cdot \text{mm}$$

**Load calculations**

Braking load:

$$L_{span} = 11907\text{mm}$$

$$a = 40\text{mm}$$

$$b = 3000\text{mm}$$

$$w = 5.5\text{m}$$

$$A_b = b \cdot a = 1.2 \times 10^5 \cdot \text{mm}^2$$

$$Q_{1k} = 300\text{kN}$$

$$q_{1k} = 9\frac{\text{kN}}{\text{m}^2}$$

$$\alpha_Q = 0.9$$

$$\alpha_{q1} = 0.7$$

$$B_{load} = 0.6 \cdot \alpha_Q \cdot \left(2 \cdot Q_{1k}\right) + 0.10 \cdot \alpha_{q1} \cdot q_{1k} \cdot w \cdot L_{span} = 365.258 \cdot kN$$

$$Q_{Bload} = \frac{B_{load}}{A_b} = 3.044 \cdot \frac{N}{mm^2}$$

Lateral load:

$$Q_{lat} = 0.25 \cdot Q_{Bload} = 0.76 \cdot \frac{N}{mm^2}$$

**Calculation of effective width**

Concept I

Deck:

$t_2 = 9mm$ top plate

$t_1 = 8mm$ bottom plate

$h_c = 120mm$

Girder:

$t_w = 17mm$

$h_w = 782mm$

$t_f = 34mm$

$b_f = 300mm$

$y_{NA.I} = 681mm$

$$y_{NA.I} = \frac{S_I}{A_I}$$

$$S_{1.I} = \left[b_{eff} \cdot t_1 + t_w \cdot h_w + \left(b_f \cdot t_f\right) \cdot 2 + b_{eff} \cdot t_2\right] \cdot y_{NA.I}$$

$$S_{2.I} = \left[\begin{array}{l} \left(b_{eff} \cdot t_1\right) \cdot \left(h_w + \frac{t_1}{2} + 2t_f\right) + t_w \cdot h_w \cdot \left(\frac{h_w}{2} + t_f\right) + \left(t_f \cdot b_f\right) \cdot \frac{t_f}{2} \ldots \\ + b_{eff} \cdot t_2 \cdot \left(h_w + 2t_f + h_c + \frac{t_1}{2}\right) + \left(t_f \cdot b_f\right) \cdot \left(h_w + t_f + \frac{t_f}{2}\right) \end{array}\right]$$

$$b_{eff.I} = \frac{\left[\begin{array}{l} -\left[t_w \cdot h_w + \left(b_f \cdot t_f\right) \cdot 2\right] \cdot y_{NA.I} + t_w \cdot h_w \cdot \left(\frac{h_w}{2} + t_f\right) + \left(t_f \cdot b_f\right) \cdot \frac{t_f}{2} \ldots \\ + \left(t_f \cdot b_f\right) \cdot \left(h_w + t_f + \frac{t_f}{2}\right) \end{array}\right]}{t_1 \cdot y_{NA.I} + t_2 \cdot y_{NA.I} - t_1 \cdot \left(h_w + \frac{t_1}{2} + 2t_f\right) - t_2 \cdot \left(h_w + 2t_f + h_c + \frac{t_1}{2}\right)} = 2.15 \cdot m$$

Concept II

$t_{top} = 9mm$

$y_{NA.II} = 555mm$

$$S_{1.II} = \left(b_{eff} \cdot t_{top} + t_w \cdot h_w + b_f \cdot t_f\right) \cdot y_{NA.II}$$

$$S_{2.II} = \left(b_{eff} \cdot t_{top}\right) \cdot \left(h_w + \frac{t_{top}}{2} + t_f\right) + t_w \cdot h_w \cdot \left(\frac{h_w}{2} + t_f\right) + \left(t_f \cdot b_f\right) \cdot \frac{t_f}{2}$$

$$b_{eff.II} = \frac{-\left(t_w \cdot h_w + b_f \cdot t_f\right) \cdot y_{NA.II} + \left[t_w \cdot h_w \cdot \left(\frac{h_w}{2} + t_f\right) + \left(t_f \cdot b_f\right) \cdot \frac{t_f}{2}\right]}{t_{top} \cdot y_{NA.II} - t_{top} \cdot \left(h_w + \frac{t_{top}}{2} + t_f\right)} = 3020\,mm$$